NASA TECHNICAL NOTE

NASA TN D-5870

NASA TN D-5870

STEADY-STATE AND STABILITY ANALYSIS OF EXTERNALLY PRESSURIZED GAS-LUBRICATED JOURNAL BEARINGS WITH HERRINGBONE GROOVES

by David P. Fleming

Lewis Research Center
Cleveland, Ohio 44135

NATIONAL AERONAUTICS AND SPACE ADMINISTRATION • WASHINGTON, D. C. • JUNE 1970

1. Report No. NASA TN D-5870	2. Government Accession No.	3. Recipient's Catalog No.
4. Title and Subtitle STEADY-STATE AND STABILITY ANALYSIS OF EXTERNALLY PRESSURIZED GAS-LUBRICATED JOURNAL BEARINGS WITH HERRINGBONE GROOVES		5. Report Date June 1970 6. Performing Organization Code
7. Author(s) David P. Fleming		8. Performing Organization Report No. E-5489
9. Performing Organization Name and Address Lewis Research Center National Aeronautics and Space Administration Cleveland, Ohio 44135		10. Work Unit No. 129-03 11. Contract or Grant No.
12. Sponsoring Agency Name and Address National Aeronautics and Space Administration Washington, D.C. 20546		13. Type of Report and Period Covered Technical Note 14. Sponsoring Agency Code
15. Supplementary Notes		

16. Abstract

A small eccentricity analysis was performed to predict load capacity and stability. Numerical results were obtained for a range of feeding parameter, pressure ratio, groove length and orifice recess volume for compressibility numbers from 0 to 50. These results were obtained from a digital computer program which is included. Results showed that the addition of herringbone grooving to an externally pressurized bearing increases stability, but reduces load capacity at low compressibility numbers. A fully grooved bearing is more stable than a partially grooved bearing. Orifice recesses reduce stability, especially at high compressibility numbers.

17. Key Words (Suggested by Author(s))	18. Distribution Statement
Gas-lubricated bearings Externally pressurized bearings Self-acting bearings Bearing stability Bearings	Unclassified - unlimited

19. Security Classif. (of this report)	20. Security Classif. (of this page)	21. No. of Pages	22. Price*
Unclassified	Unclassified	41	$3.00

*For sale by the Clearinghouse for Federal Scientific and Technical Information
Springfield, Virginia 22151

STEADY-STATE AND STABILITY ANALYSIS OF EXTERNALLY PRESSURIZED GAS-LUBRICATED JOURNAL BEARINGS WITH HERRINGBONE GROOVES

by David P. Fleming

Lewis Research Center

SUMMARY

A small eccentricity analysis was performed to predict the load capacity and stability of an externally pressurized bearing with herringbone grooves. Numerical results were obtained for a range of feeding parameters, pressure ratios, groove lengths, and orifice recess volumes for compressibility numbers from 0 to 50. These results were obtained from the digital computer program which is presented in an appendix. Results showed that the addition of herringbone grooving to an externally pressurized bearing increases stability, but reduces load capacity at low compressibility numbers. A fully grooved bearing is more stable than a partially grooved bearing. Load capacity and stability decrease near the speed where the pressure due to the herringbone groove pumping equals the external supply pressure. Orifice recesses decrease stability, particularly at high compressibility numbers.

INTRODUCTION

Gas-lubricated bearings may be divided into two broad classifications: self-acting and externally pressurized. In a self-acting bearing, the film pressure which supports the load is developed by the relative motion of the bearing parts and is proportional to the fluid viscosity. When there is no motion, the load capacity is zero. In contrast, in an externally pressurized bearing, lubricant gas under pressure is supplied from an external source. Thus, this type of bearing can have a substantial load capacity even when it is stationary.

Because of the low viscosity of gases, self-acting gas-lubricated bearings will carry a much smaller load than oil-lubricated bearings. For the same reason, they are much more susceptible to self-excited instability, commonly known as fractional frequency whirl. A major part of the research in gas-lubricated bearings has been directed toward

development of bearing configurations that will operate stably. Some of these designs, for example, tilting pad bearings, achieve stability at the expense of steady-state load capacity. One type of self-acting bearing that has good stability and can also carry a higher load than a plain bearing is the herringbone grooved bearing (refs. 1 to 3). Externally pressurized bearings also have a higher load capacity than plain self-acting bearings and also are fairly stable (ref. 4).

The principal disadvantage of the externally pressurized bearing is the need for a continuous supply of pressurized gas. The herringbone bearing, on the other hand, needs no external supply, but has no load capacity at zero speed. The two bearing types could be combined; for example, a herringbone grooved rotor could be installed in an externally pressurized bearing. External pressurization could be used for a startup; upon reaching operating speed the external supply could be shut off, and the unit operated as a self-acting herringbone bearing. Alternatively, the external supply could be maintained; the inward pumping of the herringbone grooves would reduce the amount of gas needed from the external supply.

Previous analyses have evaluated the load capacity and stability of herringbone grooved bearings (refs. 1 and 2) and of externally pressurized bearings (refs. 4 to 6). Vohr and Chow determined the load capacity of herringbone grooved bearings in reference 1; their analysis was used to evaluate stability in reference 2. Experimental stability data for herringbone bearings were obtained in reference 3. The data showed that the analysis predicts the onset of instability consistently; however, actual instability occurred at somewhat lower speeds than predicted.

The load capacity of externally pressurized bearings was determined by Lund in reference 5. In a later report (ref. 6), Lund calculated the stability of externally pressurized bearings operating at finite eccentricities. Here he included the effect of orifice recess volume and attempted to account for there being a finite number of orifices, rather than the line source usually assumed. Reference 4 evaluated the stability of an unloaded externally pressurized bearing and included the effect of orifice recess volume as in reference 6.

All of these analyses are similar in that they use a small eccentricity perturbation and solve for the perturbed pressure using a separation of variables scheme. Thus it is easy, in principle, to combine the solutions to find the load capacity and stability of a herringbone bearing with external pressurization.

The objectives of this investigation are to determine analytically the steady-state and stability characteristics of externally pressurized herringbone grooved bearings. Various combinations of supply pressure, feeding parameter, orifice recess volume, and groove length will be explored.

ANALYSIS

The bearing configuration to be analyzed is shown in figure 1. It consists of a double row externally pressurized bearing with herringbone grooves. The grooves are shown on the rotor, but the analysis is unchanged if they are on the bearing. The herringbone grooves may be partial, as shown, or they may extend the full length of the bearing. For simplicity of presentation, it will be assumed that the rows of orifices are closer to the midplane of the bearing than are the herringbone grooves. This includes the limiting case of the orifice rows coinciding with the ends of the grooves. Extension to other cases is straightforward. It will be further assumed that the bearing is symmetric about the midplane. With this assumption, only half the bearing need be analyzed. Other assumptions are that the number of herringbone grooves is large (ref. 1) and that there are enough orifices so that each row may be approximated by a line source.

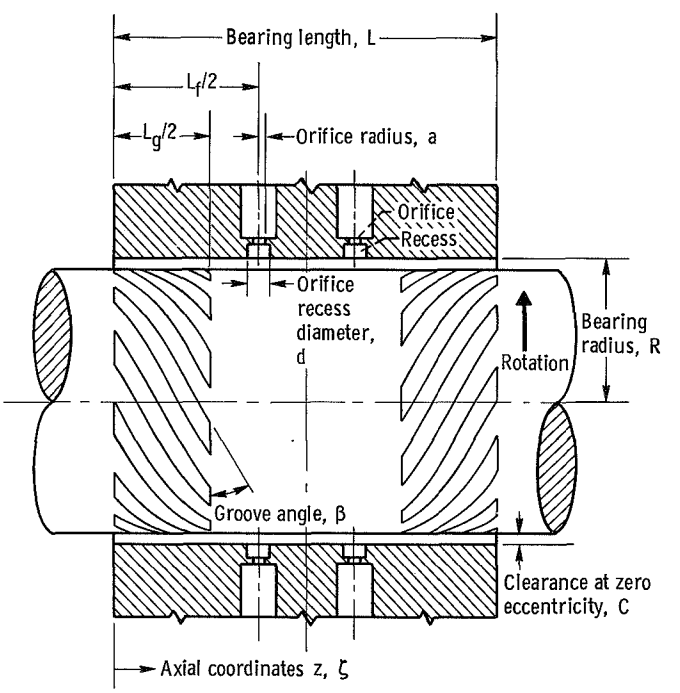

Figure 1. - Externally pressurized herringbone bearing.

The analysis of reference 1 applies, with the exception that the axial mass flow is no longer zero as it was in the herringbone bearing without orifices. Thus, the differential equations and boundary conditions must be modified to account for axial mass flow in the bearing and flow through the orifice.

To conveniently obtain solutions for steady whirling, which are needed for the stability analysis, a rotating coordinate system is introduced by

$$\theta^* = \theta - \omega_p t \tag{1}$$

where ω_p is the frequency of steady circular whirling. Symbols are defined in appendix A. The differential equation to be solved (from ref. 1), is

$$\frac{1}{R}\frac{\partial}{\partial\theta^*}\left[\mathscr{M}_{\theta r}\sin\beta + (\mathscr{M}_{zg} - \mathscr{M}_{zr})\,\alpha\cos\beta - \rho R\omega h_r \sin\beta\right] + \frac{\partial}{\partial z}\left[\alpha\mathscr{M}_{zg} + (1-\alpha)\mathscr{M}_{zr}\right]\sin\beta$$

$$+ (\omega - \omega_p)\frac{\partial}{\partial\theta^*}\left[\rho\alpha h_g - \rho(1-\alpha)h_r\right]\sin\beta = 0 \tag{2}$$

This and subsequent expressions were derived for the herringbone grooved section of the bearing, but may also be used for the smooth section by setting $h_g = h_r$. The expressions for the mass flows $\mathscr{M}_{\theta r}$, $\mathscr{M}_{zg}$, and $\mathscr{M}_{zr}$ are in appendix B. The procedure now is to approximate the film pressure according to

$$p(\theta^*, z) \sim p_0(z) + \epsilon p_1(\theta^*, z) \tag{3}$$

Equation (3) and the expressions for the mass flows from appendix B are substituted into equation (2). The resulting expression is considered an identity in the eccentricity ratio ϵ, and a separate equation written for each power of ϵ which appears. Powers of ϵ higher than 1 are neglected; thus, two equations result. The zero-order equation can be written

$$\frac{d}{dz}\left[\alpha\mathscr{M}_{zg0} + (1-\alpha)\mathscr{M}_{zr0}\right] = 0 \tag{4}$$

This may be integrated once immediately to yield

$$\alpha\mathscr{M}_{zg0} + (1-\alpha)\mathscr{M}_{zr0} = \mathscr{M}_{z0} = \text{Constant} \tag{5}$$

In terms of the dimensionless pressure $P_0 = p_0/p_a$ and dimensionless coordinate $\zeta = z/L$, equation (5) for an isothermal bearing becomes

$$P_0\left[\mathscr{C}_p - \frac{dP_0}{d\zeta}\right] = \frac{12\mu\mathscr{R}T\mathscr{M}_{z0}R}{C^3 p_a^2 \mathscr{C}_1} = \text{Constant} \tag{6}$$

The first-order equation is

$$\frac{\partial^2 P_1}{\partial \zeta^2} + \left[2\frac{dP_0}{d\zeta} - \mathscr{C}_p\right]\frac{\partial P_1}{\partial \zeta} + \mathscr{C}_3 P_0 \frac{\partial^2 P_1}{\partial \zeta\, \partial \theta^*} + \left[\mathscr{C}_{4a}\frac{dP_0}{d\zeta} + \mathscr{C}_{4b}(\Lambda - \sigma) + \mathscr{C}_{4c}\right]\frac{\partial P_1}{\partial \theta^*} + \mathscr{C}_5 P_0 \frac{\partial^2 P_1}{\partial \theta^{*2}}$$

$$+ \left[\mathscr{C}_{6a}\frac{dP_0}{d\zeta} + \mathscr{C}_{6b}(\Lambda - \sigma) + \mathscr{C}_{6c}\right] P_0 \sin\theta^* + \mathscr{C}_7 \frac{dP_0}{d\zeta}\cos\theta^*$$

$$+ \left[\mathscr{C}_p - \frac{dP_0}{d\zeta}\right]\frac{dP_0}{d\zeta}\cdot\frac{1}{P_0} = 0 \tag{7}$$

where the $\mathscr{C}$'s are constants given in appendix B. They differ from the constants given in reference 1 because $dP_0/d\zeta$ is not constant in a bearing with orifices. The constant Λ is the standard gas bearing compressibility number, and σ is a dimensionless representation of the whirl frequency.

Boundary conditions. - At the ends of the bearing

$$P_0 = 1$$

and

$$P_1 = 0 \tag{8}$$

At the bearing midplane, by symmetry,

$$\frac{dP_0}{d\zeta} = \frac{\partial P_1}{\partial \zeta} = 0 \tag{9}$$

Pressures P_0 and P_1 are continuous throughout the bearing film, but there will be discontinuities in the derivatives $dP_0/d\zeta$ and $\partial P_1/\partial \zeta$. These are caused at $\zeta = \zeta_g$, by the end of the herringbone groove pattern, and at $\zeta = \zeta_f$, by the gas flow through the orifices.

Since, in differential equation (6) for P_0, $dP_0/d\zeta$ is the highest order derivative, the discontinuity in $dP_0/d\zeta$ at $\zeta = \zeta_g$ need not be found explicitly. The discontinuity in $\partial P_1/\partial \zeta$ at $\zeta = \zeta_g$ may be determined by noting that $\mathscr{M}_{z1} = \alpha\mathscr{M}_{zg1} + (1 - \alpha)\mathscr{M}_{zr1}$ is continuous at this point. The perturbed mass flows $\mathscr{M}_{zg1}$ and $\mathscr{M}_{zr1}$ may be found by differentiating the expressions for $\mathscr{M}_{zg}$ and $\mathscr{M}_{zr}$ (appendix B) with respect to ϵ and

then setting $\epsilon = 0$, for example, $\mathscr{M}_{zg1} = \partial \mathscr{M}_{zg}/\partial\epsilon\big|_{\epsilon=0}$. The result for $\partial P_1/\partial\zeta$ is

$$\left.\frac{\partial P_1}{\partial \zeta}\right|_{\zeta=\zeta_g^+} = \mathscr{M}_{z0}\frac{12\mu\mathscr{R}TL}{P_0C^3p_a^2}\mathscr{C}_m\cos\theta^* + \mathscr{C}_1\frac{L}{R}\left[\mathscr{C}_7\cos\theta^* + \frac{1}{2}\mathscr{C}_3\frac{\partial P_1}{\partial\theta^*} + \left.\frac{\partial P_1}{\partial\zeta}\right|_{\zeta=\zeta_g^-}\right] \tag{10}$$

in which ζ_g^+ denotes a value of ζ infinitesimally greater than ζ_g. The expression for $\mathscr{C}_m$, as well as for the other $\mathscr{C}$'s, is in appendix B.

At the orifices, conditions are similar to those in an ungrooved externally pressurized bearing, analyzed in reference 5. One important difference is that, in an externally pressurized herringbone bearing, the gas flow through the orifices can be in either direction, depending on the supply pressure and the pumping in the herringbone grooves. Boundary conditions on pressure are found by balancing the gas flow through the orifices with that through the bearing film. The results are

$$m_0 = -\frac{DP_{0c}}{L\Lambda_t}\left.\frac{dP_0}{d\zeta}\right|_{\zeta=\zeta_f^-} \tag{11}$$

and

$$P_{0c}\left[\left.\frac{\partial P_1}{\partial\zeta}\right|_{\zeta=\zeta_f^-} - \left.\frac{\partial P_1}{\partial\zeta}\right|_{\zeta=\zeta_f^+}\right] = -m_0\Lambda_t\frac{L}{D}\left[\left.\frac{P_{1c}}{m_0P_s}\frac{\partial m}{\partial\left(\frac{P_c}{P_s}\right)}\right|_{\epsilon=0} - \frac{3+2\delta^2}{1+\delta^2}\cos\theta^* - \frac{P_{1c}}{P_{0c}}\right] + 2P_{0c}\sigma\psi_1\frac{L}{D}\frac{\partial P_{1c}}{\partial\theta^*} \tag{12}$$

The dimensionless mass flow m is given by the usual orifice flow equations, with inherent compensation effects accounted for as in reference 6.

$$m = \mathscr{M}_z\frac{4R\sqrt{\mathscr{R}T}\sqrt{1+\left(\frac{\delta C}{h_r}\right)^2}}{Na^2p_a} \tag{13}$$

$$
\left.
\begin{aligned}
m &= \alpha_d P_s \sqrt{\frac{2k}{k+1}} \left(\frac{2}{k+1}\right)^{1/(k-1)} && \frac{P_c}{P_s} \le \left(\frac{2}{k+1}\right)^{k/(k-1)} \\
m &= \alpha_d P_s \sqrt{\frac{2k}{k-1}} \left(\frac{P_c}{P_s}\right)^{1/k} \sqrt{1 - \left(\frac{P_c}{P_s}\right)^{(k-1)/k}} && 1 \ge \frac{P_c}{P_s} > \left(\frac{2}{k+1}\right)^{k/(k-1)} \\
m &= \alpha_d P_c \sqrt{\frac{2k}{k-1}} \left(\frac{P_s}{P_c}\right)^{1/k} \sqrt{1 - \left(\frac{P_s}{P_c}\right)^{(k-1)/k}} && 1 > \frac{P_s}{P_c} > \left(\frac{2}{k+1}\right)^{k/(k-1)} \\
m &= \alpha_d P_c \sqrt{\frac{2k}{k+1}} \left(\frac{2}{k+1}\right)^{1/(k-1)} && \frac{P_s}{P_c} \le \left(\frac{2}{k+1}\right)^{k/(k-1)}
\end{aligned}
\right\} \qquad (14)
$$

The flow when the bearing is concentric, m_0; is obtained by using the concentric values $P_c = P_{0c}$ and $h_r = C$ in equations (13) and (14). The feeding parameter Λ_t (eqs. (11) and (12)) is defined by

$$\Lambda_t = \frac{6\mu N_a^2 \sqrt{\mathscr{R}T}}{p_a C^3 \sqrt{1+\delta^2}} \qquad (15)$$

and ψ_1 (in eq. (12)) by

$$\psi_1 = \frac{NV}{\pi DLC} \cdot \frac{L}{P_{0c} D} = \frac{vL}{P_{0c} D} \qquad (16)$$

Solution of differential equations. - The constant in equation (6) is determined by the gas flow through the orifices. From equation (13), with $\epsilon = 0$,

$$\mathscr{M}_{z0} = \frac{N_a^2 p_a m_0}{4R\sqrt{\mathscr{R}T}\sqrt{1+\delta^2}} \qquad (17)$$

Combination of equations (15) and (17) with equation (6) gives

$$\frac{dP_0}{d\zeta} - \mathscr{C}_p = -\frac{m_0 \Lambda_t}{2P_0 \mathscr{C}_1} \tag{18}$$

This differential equation contains two unknowns: the pressure P_0 and the mass flow m_0. The procedure for determining P_0 and m_0 is (1) assume a value for m_0, (2) integrate equation (18) from $\zeta = 0$ to $\zeta = \zeta_f$, using a forward integration scheme such as Runge-Kutta (for $\zeta > \zeta_f$, $\mathscr{M}_{z0} = 0$ and $P_0 = P_{0c}$), (3) calculate a new value of m_0 from the value of $P_0 = P_0(\zeta_f)$ just found, and (4) compare with the previous m_0; if different, repeat steps 2 to 4 until convergence is obtained.

Differential equation (7) for P_1 may be solved (as in ref. 2) by assuming that P_1 is represented by

$$P_1 = \mathcal{R}e\left[G(\zeta)e^{i\theta^*}\right] \tag{19}$$

When this is substituted into equation (7) there results

$$\frac{d^2G}{d\zeta^2} + \left(2\frac{\partial P_0}{d\zeta} - \mathscr{C}_p\right)\frac{dG}{d\zeta} + i\mathscr{C}_3 P_o \frac{dG}{d\zeta} + \left[\mathscr{C}_{4a}\frac{dP_0}{d\zeta} + \mathscr{C}_{4b}(\Lambda - \sigma) + \mathscr{C}_{4c}\right] iG - \mathscr{C}_5 P_0 G$$

$$- \left[\mathscr{C}_{6a}\frac{dP_0}{d\zeta} + \mathscr{C}_{6b}(\Lambda - \sigma) + \mathscr{C}_{6c}\right] iP_0 + \mathscr{C}_7 \frac{dP_0}{d\zeta} + \frac{1}{P_0}\left(\mathscr{C}_p - \frac{dP_0}{d\zeta}\right)\frac{dP_0}{d\zeta} = 0 \tag{20}$$

Boundary conditions for P_1 in equations (8), (9), (10), and (12) transform into the following boundary conditions for G

$$G = 0 \qquad \text{at} \quad \zeta = 0 \tag{21}$$

$$\frac{dG}{d\zeta} = 0 \qquad \text{at} \quad \zeta = \frac{1}{2} \tag{22}$$

$$\left.\frac{dG}{d\zeta}\right|_{\zeta=\zeta_g^+} = \frac{\Lambda_t m_0 L \mathscr{C}_m}{2P_0 R} + \mathscr{C}_1 \frac{L}{R}\left(\mathscr{C}_7 + \frac{1}{2}\mathscr{C}_3 iG\Big|_{\zeta=\zeta_g} + \left.\frac{dG}{d\zeta}\right|_{\zeta=\zeta_g^-}\right) \tag{23}$$

$$\left.\frac{dG}{d\zeta}\right|_{\zeta=\zeta_f^+} = \left.\frac{dG}{d\zeta}\right|_{\zeta=\zeta_f^-} - \frac{L}{R} G_c\left(\frac{\psi_0}{P_s} + \frac{m_0 \Lambda_t}{2P_{0c}^2} + i\sigma\psi_1\right) + \frac{1.5 + \delta^2}{1 + \delta^2}\frac{m_0 \Lambda_t}{P_{0c} R} \tag{24}$$

The perturbed pressure P_1 may now be determined by solving differential equation (20) numerically by the method detailed in reference 4.

Determination of load and stability. - The radial and tangential components of the bearing load are found by integrating the film pressure over the bearing area.

$$\begin{Bmatrix} F_r \\ F_t \end{Bmatrix} = \int_0^L \int_0^{2\pi} p_a P \begin{Bmatrix} -\cos\theta^* \\ \sin\theta^* \end{Bmatrix} R \, d\theta^* \, dz$$

Substitution of equations (3) and (19) for P and performance of the θ^* integration yields, in dimensionless variables,

$$\begin{Bmatrix} f_r \\ f_t \end{Bmatrix} = -\pi \begin{Bmatrix} Re \\ Im \end{Bmatrix} \int_0^{1/2} G \, d\zeta \tag{25}$$

The dimensionless forces in equation (25) are defined by

$$\left.\begin{aligned} f_r &= \frac{F_r}{\epsilon p_a LD} \\ f_t &= \frac{F_t}{\epsilon p_a LD} \end{aligned}\right\} \tag{26}$$

The resultant bearing load $\overline{W}$ and attitude angle φ may now be calculated.

$$\overline{W} = \frac{W}{\epsilon p_a LD} = \left(f_r^2 + f_t^2\right)^{1/2} \tag{27}$$

$$\varphi = \tan^{-1}\left(\frac{f_t}{f_r}\right) \tag{28}$$

Figure 2 illustrates the relations among these quantities.

When the bearing is operating stably, the frequency number σ is zero. To determine the threshold of instability, σ is varied until $f_t = 0$ (ref. 7). The bearing neutral stability condition is then found by equating the centrifugal force, due to the whirling bearing mass, to the radial bearing force.

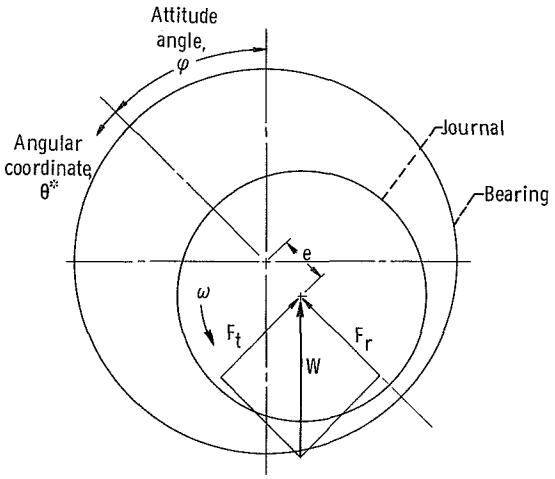

Figure 2. - Notation for eccentric bearing.

$$Me\omega_{pn}^2 = F_{rn} \tag{29}$$

The subscript n denotes the condition where $f_t = 0$.

A dimensionless bearing mass may be defined by

$$\overline{M} = \frac{Mp_a}{2L\mu^2}\left(\frac{C}{R}\right)^5 \tag{30}$$

In terms of previously calculated quantities, $\overline{M}$ for the neutral stability condition is given by

$$\overline{M}_n = \frac{144\, f_{rn}}{\sigma^2} \tag{31}$$

Reference 7 shows that $\overline{M}_n$ is an upper limit of $\overline{M}$ for stability if the quantity $\partial f_t/\partial\sigma$ is negative at $\sigma = \sigma_n$; conversely, $\overline{M}_n$ is a lower limit for stability if $\partial f_t/\partial\sigma$ is positive at $\sigma = \sigma_n$.

RESULTS AND DISCUSSION

The analysis of the preceding section has been used to obtain steady-state and stability information for a number of externally pressurized herringbone bearing configura-

tions. Results were obtained using the computer program presented in appendix C. The computer program was checked by running cases for a plain externally pressurized bearing (without grooves) and a herringbone grooved bearing (without orifices). Results for the test cases agreed well with those of reference 1 and 4.

Because of the large number of parameters that may vary in a bearing, the effects of all of them were not investigated. Rather, a number of the parameters were fixed. The basic bearing chosen for study has a length to diameter ratio of 1 with a single row of orifices at the bearing midplane. No inherent compensation effects were included. The herringbone groove angle β is 30°; the groove width fraction α, 0.5; and the groove clearance to land clearance ratio H, 2.1. These values approximate the optima found in reference 1 for maximizing the radial load component. Three groove length fractions L_g/L were investigated: 0 (ungrooved), 0.5, and 1 (fully grooved). The feeding parameter Λ_t was varied from 0 (no orifices) to 4, and the supply pressure ratio from 1 to 5. Any other configurations of interest can be easily investigated using the computer program in appendix C.

Steady State Results

Figure 3 shows the effect of the feeding parameter Λ_t on load capacity. Figure 3(a) is for a pressure ratio P_s of 1, which means the bearing is actually unpressurized. For this case, the load capacity $\overline{W}$ is greatest when there are no orifices ($\Lambda_t = 0$); $\overline{W}$ decreases with increasing Λ_t. A partially grooved bearing will carry a higher load than a fully grooved bearing. The ungrooved bearing is not shown for this case; it is unsuitable for most uses because it is unstable when not loaded.

Figure 3(b), for a pressure ratio of 2, shows that at low values of Λ (less than about 5) the load capacity now increases with increasing feeding parameter Λ_t. At higher Λ's the order is reversed for the grooved bearings. That is, load capacity decreases with increasing Λ_t, as was the case for the unpressurized bearing. The load capacity of the partially grooved bearing again exceeds that of the fully grooved bearing. For Λ less than 13 to 33 (depending on feeding parameter) the ungrooved bearing has the highest load capacity. At higher Λ, the load curves for the ungrooved bearings level off, while those for the grooved bearings continue to rise. This, of course, is because of the increasing self-pressurization by the inward pumping herringbone grooves.

The load curves for the grooved bearings show an interesting phenomenon in that they have a pronounced depression at an intermediate value of Λ. This depression occurs when the pumping of the herringbone grooves raises the pressure on the bearing side of the orifices to the pressure that is supplied externally. Near this point, the derivative of mass flow with respect to bearing orifice pressure P_c becomes very large

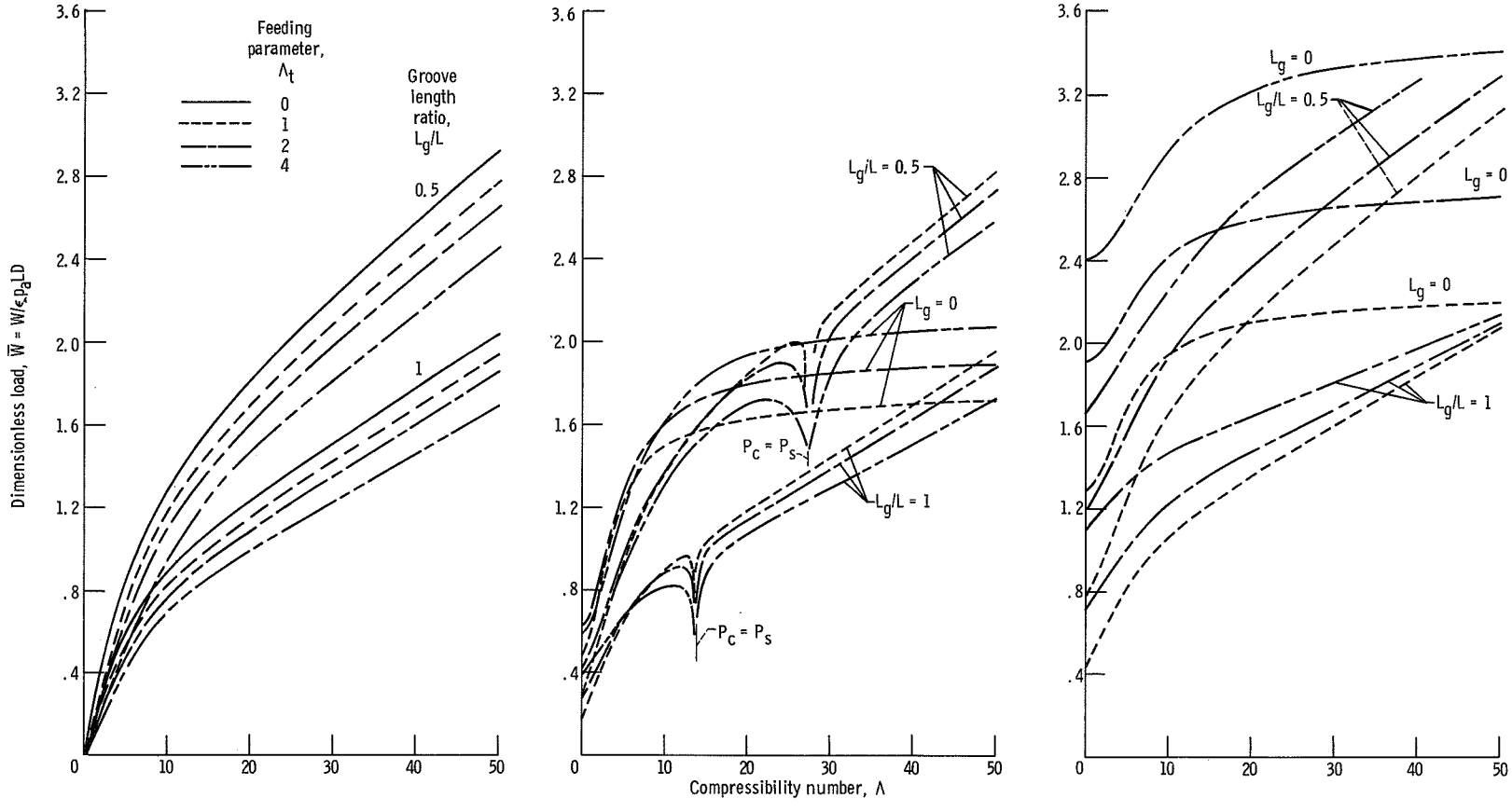

Figure 3. - Effect of feeding parameter Λ_t on load. Length to diameter ratio, 1; orifice location parameter L_f/L, 1; groove angle, 30°; groove width fraction, 0.5; groove to land clearance ratio, 2.1.

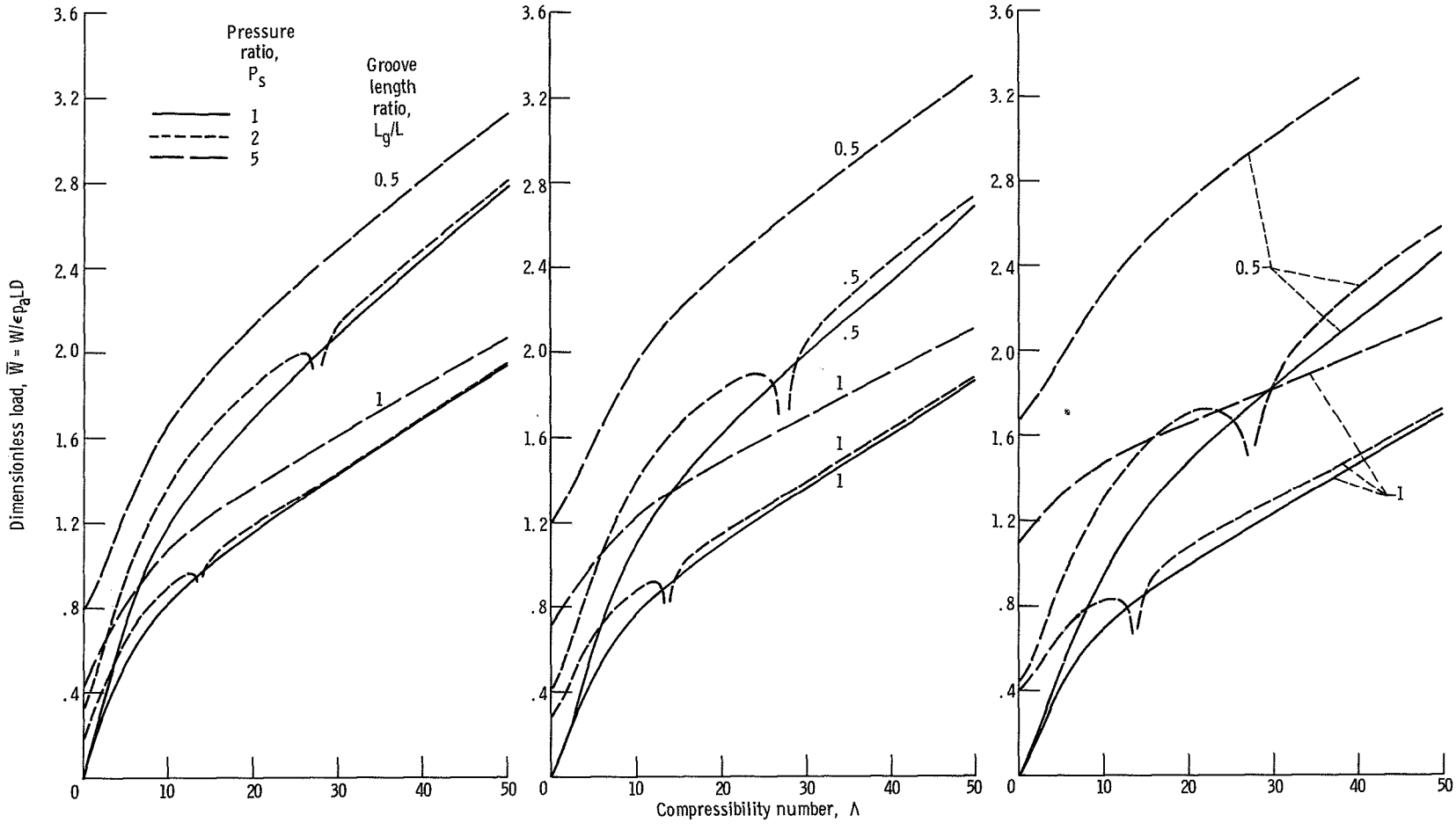

Figure 4. - Effect of pressure ratio on load. Length to diameter ratio, 1; orifice location parameter L_f/L, 1; groove angle, 30°; groove width fraction, 0.5; groove to land clearance ratio, 2.1.

(eq. (14)). That is, a very small change in P_c causes a large change in orifice flow. Consequently, the bearing is not as well compensated and the stiffness is reduced.

It should be pointed out that for an actual bearing the loss of load capacity will not be as great as predicted by figure 3(b). This is because the difference $\Delta m/\Delta(P_c/P_s)$ for finite $\Delta(P_c/P_s)$ does not approach the infinite value of the derivative $\partial m/\partial(P_c/P_s)$. Also, the orifice flow equations (14) neglect viscous effects. These become significant at low flow rates and reduce the value of $\partial m/\partial(P_c/P_s)$ near $P_c = P_s$.

Load curves for a pressure ratio of 5 are plotted in figure 3(c). The trends of figures 3(a) and (b) are continued here. Load capacity increases with increasing Λ_t out to the highest compressibility number plotted. No depressions occur in the curves (as in fig. 3(b)), because the Λ value where $P_c = P_s$ is beyond the boundary of the figure.

Figures 3(b) and (c) show that the addition of grooves to an externally pressurized bearing lowers the load capacity at low compressibility numbers, but at higher Λ the load can be increased. The compressibility number, where the load capacity of the grooved bearing first becomes greater than that of the ungrooved bearing, varies with the pressure ratio, length of grooves, and feeding parameter.

The effect of pressure ratio on load is shown in figure 4. Load capacity generally increases with pressure ratio. The load capacity for $P_s = 2$ is little different than for $P_s = 1$ (unpressurized), particularly at higher compressibility numbers. Near the value of Λ where $P_c = P_s$ (depression in load curve), the load capacity for $P_s = 2$ can drop below that for $P_s = 1$. Increasing the pressure ratio to 5 results in a relatively large increase in load capacity, particularly at low compressibility numbers and large feeding parameters.

Attitude angles are plotted in figure 5 for a pressure ratio of 2. Except at quite low compressibility numbers ($\Lambda < 5$), attitude angles are smaller for smaller values of the feeding parameter Λ_t. The grooved bearings (figs. 5(b) and (c)) exhibit behavior generally similar to an ungrooved externally pressurized bearing, with two exceptions. At zero speed ($\Lambda = 0$) the grooved bearings have a small attitude angle, which may be positive or negative, depending on the length of the grooves. In addition, when the pumping of the herringbone grooves increases the pressure P_c to near the supply pressure P_s, the attitude angle rises rapidly. This corresponds to the drop in load capacity mentioned earlier. A comparison of figures 5(a) to (c) shows that attitude angle decreases with increasing groove length, except at high compressibility numbers ($\Lambda > 35$), where the bearing with half-length grooves has a lower attitude angle than either the fully grooved or ungrooved bearing.

Because the herringbone grooves act as a pump, the gas pressure in the bearing increases with increasing compressibility number. Figure 6 shows the pressure at the center of the bearing, P_{0c}, for three values of the feeding parameter Λ_t, at an external

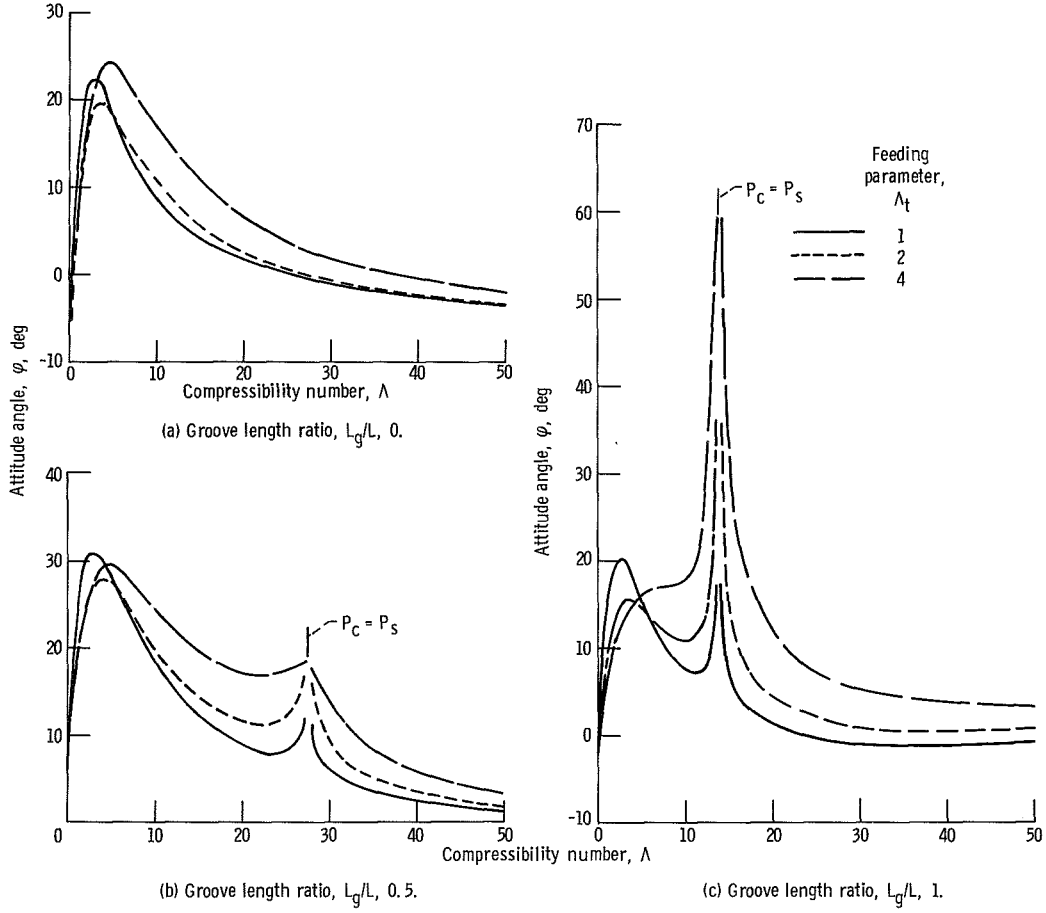

Figure 5. - Effect of feeding parameter on attitude angle. Pressure ratio P_s, 2; length to diameter ratio, 1; orifice location parameter L_f/L, 1; groove angle, 30°; groove width fraction, 0.5; groove to land clearance ratio, 2.1.

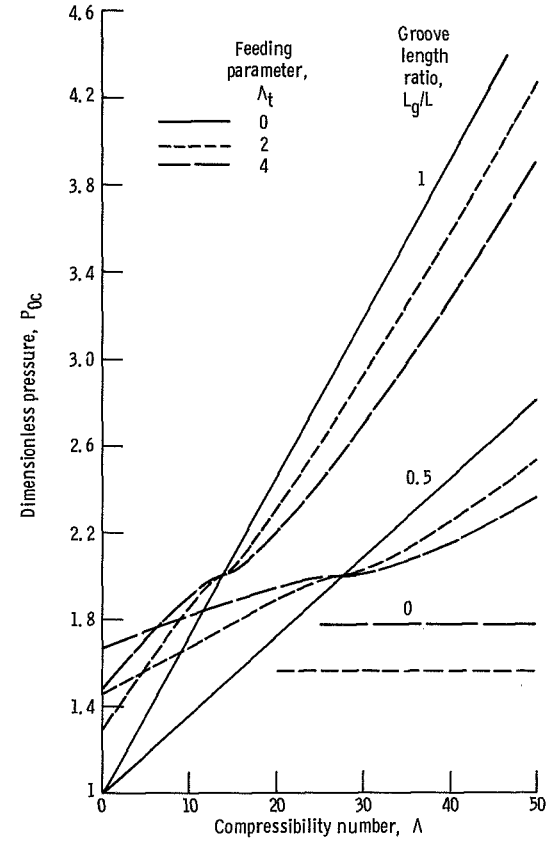

Figure 6. - Pressure at center of bearing. Pressure ratio, 2; length to diameter ratio, 1; orifice location parameter L_f/L, 1; groove angle, 30°; groove width fraction, 0.5; groove to land clearance ratio, 2.1.

supply pressure ratio of 2. As expected, larger values of Λ_t decrease the rate of change of P_{0c} with Λ. This is because a larger Λ_t means the bearing is more open to the external supply. The fully grooved bearing's pressure changes more rapidly than does the partially grooved, since pumping is proportional to groove length. Pressure does not change with compressibility number in the ungrooved bearings; to avoid confusion, these curves have not been extended to $\Lambda = 0$. The solid lines, for $\Lambda_t = 0$, indicate the pressure in a bearing with no orifices; they are, of course, valid for any supply pressure.

The gas mass flow through the bearing appears in figure 7 for the same bearing conditions as in figure 6. There are additional curves for $\Lambda_t = 1$. For $\Lambda_t = 0$, the mass flow is always 0. A negative value of m_0 indicates the gas flow is from the pressurized

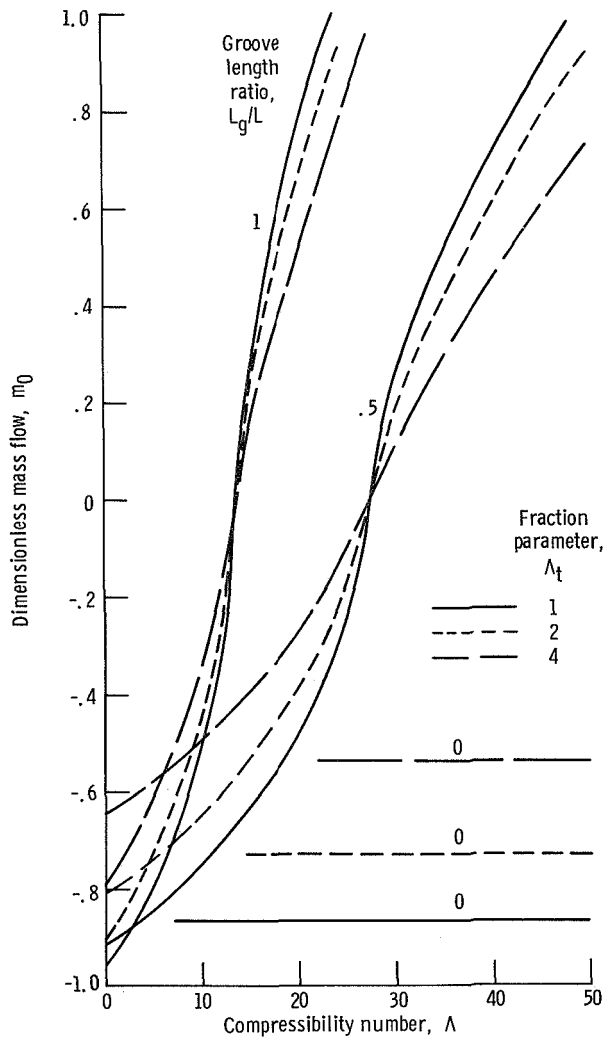

Figure 7. - Gas flow through bearing. Pressure ratio P_s, 2; length to diameter ratio, 1; orifice location parameter L_f/L, 1; groove angle, 30°; groove width fraction, 0.5; groove to land clearance ratio, 2.1.

supply to the bearing, whereas positive m_0 indicates the bearing is pumping gas into the pressurized supply.

The mass flow curves are arranged in the same order as the bearing pressure curves of figure 6. Note that the magnitude of the dimensionless flow m_0 decreases as the feeding parameter increases. This is due to the way mass flow is made dimensionless. At zero speed ($\Lambda = 0$), gas consumption increases with increasing length of grooves. This is because a grooved portion of a bearing has a larger flow area, and thus offers less resistance than an ungrooved portion.

Stability Results

In order to keep the figures presented to a reasonable number, stability information will not be given for all combinations of groove length, pressure ratio, feeding parameter, and orifice recess volume which were investigated. Instead, the basic bearing mentioned at the beginning of this section will be further defined, and results presented for variations of each of the preceding four parameters from their basic values. These basic values are $L_g/L = 1$, $P_s = 2$, $\Lambda_t = 2$, and $v = 0$.

Figure 8 shows the variation of stability with compressibility number, with groove length as a parameter. Stability, as measured by the dimensionless mass $\overline{M}$, generally decreases with increasing Λ, and increases with groove length. Above a compressibility number of 15, the stability of the fully grooved bearing increases sharply and becomes much greater than that of either the half-grooved or ungrooved bearing.

The stability curves of the fully grooved and half-grooved bearings have distinct depressions near $\Lambda = 14$ and $\Lambda = 27$, respectively. These depressions correspond to the depressions in the load curves of figures 3(b) and 4(b). As was discussed regarding the load capacity curves, the drop in stability in an actual bearing whirling with a finite eccentricity would probably not be as drastic as figure 8 predicts. With an actual bearing, problems with this low stability region can probably be avoided by passing through the region rapidly, either by accelerating the bearing rotor or changing the supply pressure.

Near a compressibility number of 38, the stability curve for the half-grooved bearing becomes very steep, in effect imposing an upper speed limit even for very small values of $\overline{M}$. This limit generally occurred between compressibility numbers of 20 and 40 in the half-grooved bearings. A similar limit was not observed for fully grooved or ungrooved bearings within the range of compressibility numbers investigated.

The effect of the feeding parameter Λ_t on stability is shown by figure 9. At low compressibility numbers ($\Lambda < 5$), higher feeding parameters give greater stability. Near $\Lambda = 14$, where the herringbone pumping pressure becomes equal to the supply

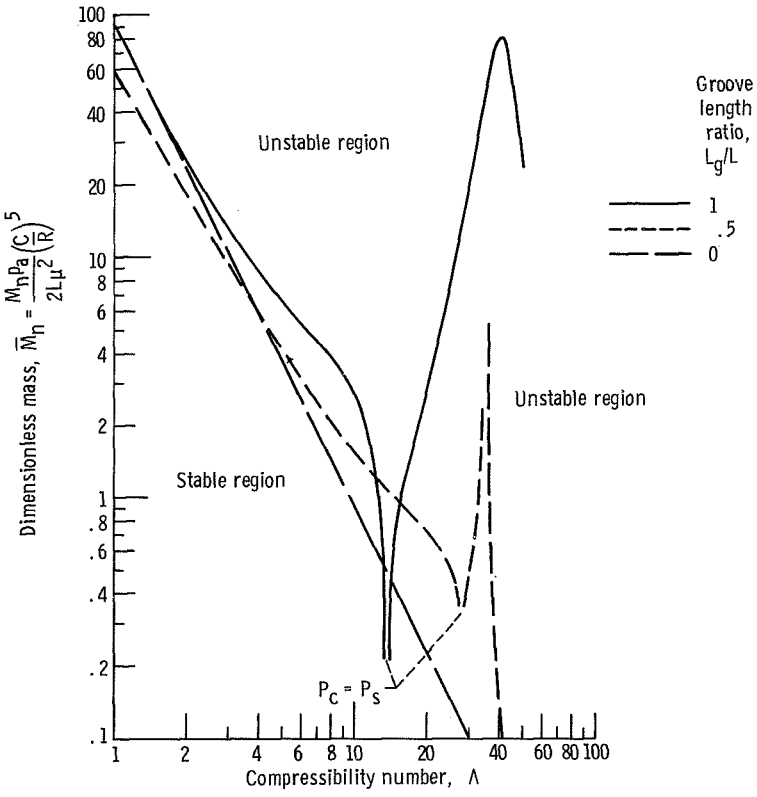

Figure 8. - Effect of groove length on stability. Pressure ratio P_s, 2; feeding parameter, 2; orifice recess volume ratio, 0; length to diameter ratio, 1; orifice location parameter L_f/L, 1; groove angle, 30°; groove width fraction, 0.5; groove to land clearance ratio, 2.1.

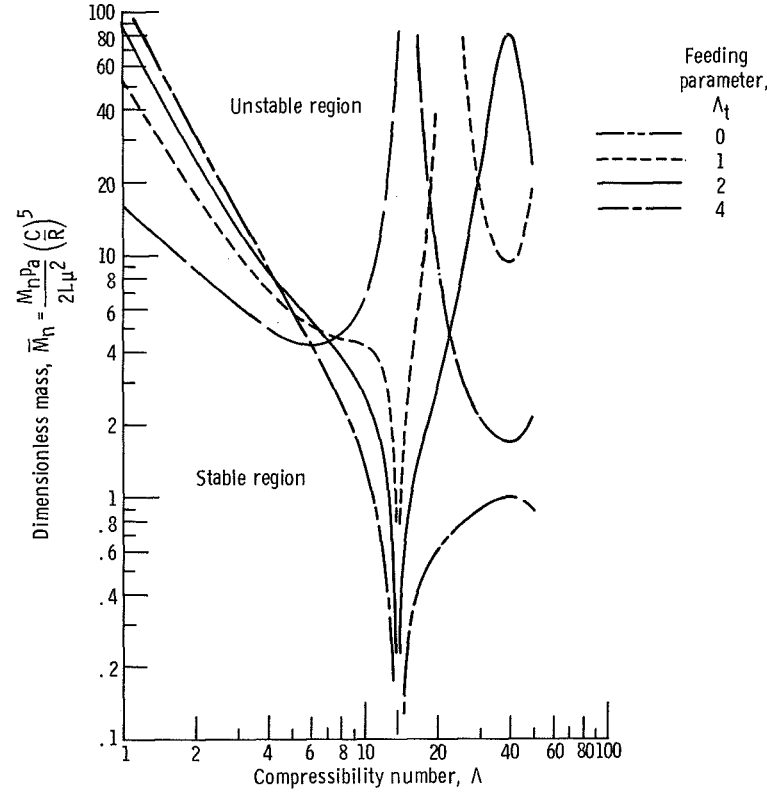

Figure 9. - Effect of feeding parameter on stability. Pressure ratio P_s, 2; groove length ratio L_g/L, 1; orifice recess volume ratio, 0; length to diameter ratio, 1; orifice location parameter L_f/L, 1; groove angle, 30°; groove width fraction, 0.5; groove to land clearance ratio, 2.1.

pressure, the order is reversed, with the no-orifice bearing ($\Lambda_t = 0$) most stable. At high Λ (>20), there is no clear trend. The greatest stability is offered by $\Lambda_t = 2$, and the least by $\Lambda_t = 4$.

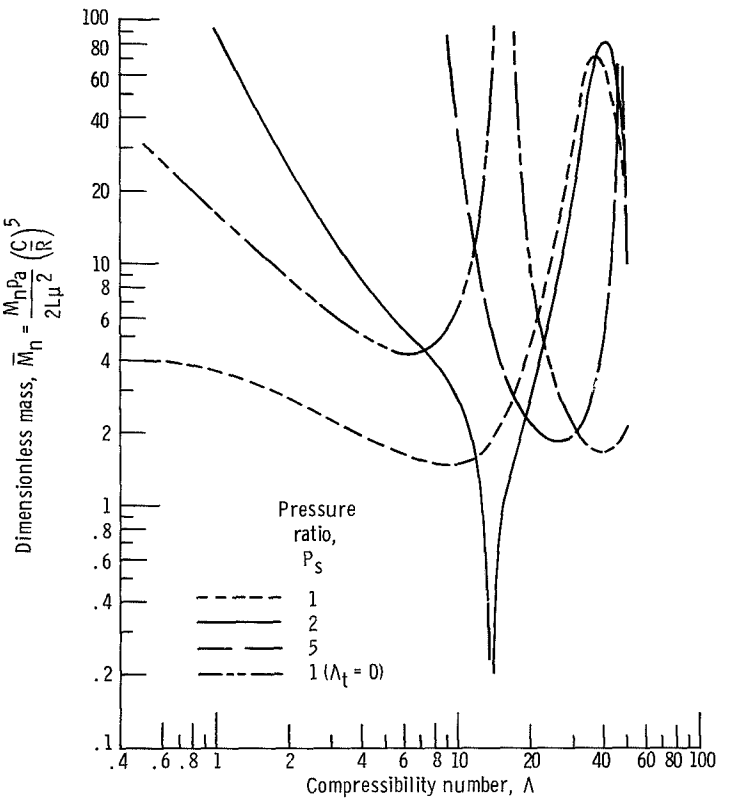

Figure 10. - Effect of pressure ratio on stability. Groove length ratio, L_g/L, 1; feeding parameter, Λ_t, 2; length to diameter ratio, 1; orifice recess volume ratio, 0; orifice location parameter L_f/L, 1; groove angle, 30°; groove width fraction, 0.5; groove to land clearance ratio, 2.1.

Figure 10 shows the effect on stability of a variation in supply pressure ratio. Included in this figure is the curve for $\Lambda_t = 0$; the remainder of the curves are for $\Lambda_t = 2$. For low compressibility numbers ($\Lambda < 10$), $P_s = 5$ provides the greatest stability; the curve is beyond the maximum ordinate of the figure. Stability decreases with decreasing pressure ratio. The plain herringbone bearing ($\Lambda_t = 0$) is between $P_s = 1$ and $P_s = 2$ ($P_s = 1$ denotes a bearing whose supply lines are open to the atmosphere). For compressibility numbers between 10 and 20 there is no clear optimum, as the curves rise and fall. At high Λ, pressure ratios of 1 and 2 are more stable than $P_s = 5$ or the no-orifice bearing. The figure shows that the addition of orifices to a herringbone bearing, without pressurization, lowers the stability at low compressibility numbers, but can increase the stability at high Λ.

The decrease in stability due to a small orifice recess is shown in figure 11. For

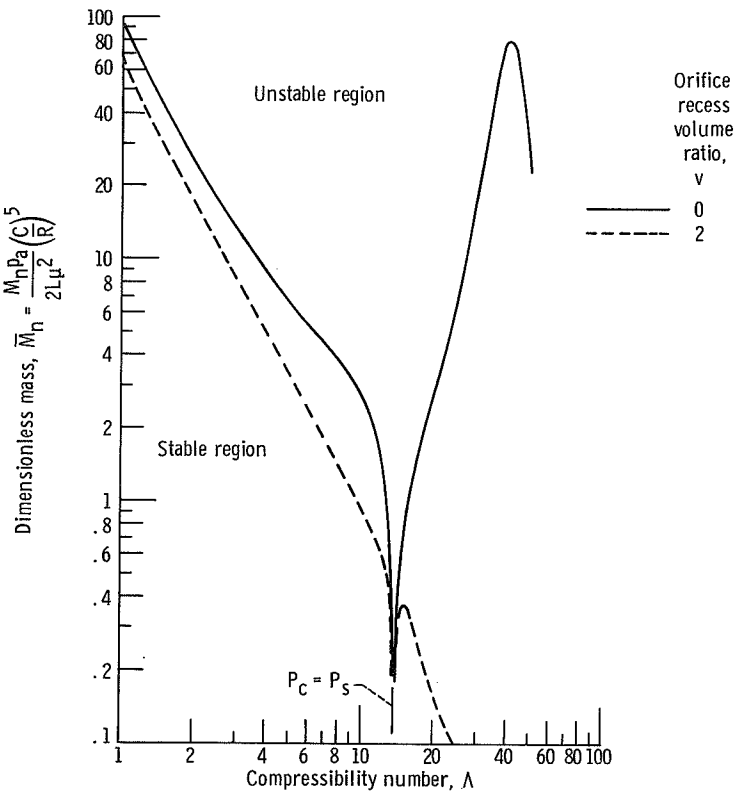

Figure 11. - Effect of recess volume on stability. Pressure ratio, 2; groove length ratio, L_g/L, 1; feeding parameter, 2; length to diameter ratio, 1; orifice location parameter L_f/L, 1; groove angle, 30°; groove width fraction, 0.5; groove to land clearance ratio, 2.1.

compressibility numbers less than 14 there is only a small loss of stability. At higher Λ, however, the stability for a recess volume ratio of 0.2 continuously decreases, while the stability for $v = 0$ increases from $\Lambda = 14$ to a maximum at $\Lambda = 40$ before decreasing. This behavior at higher compressibility numbers is typical of the effect of recess volume on the bearing configurations studied.

Multibranch curves. - For all cases of finite recess volume in grooved bearings, there was more than one neutral stability condition found at the higher compressibility numbers. That is, for a given Λ, there was more than one whirl frequency which yielded $f_t = 0$. Figure 12 illustrates this for a feeding parameter of 2, pressure ratio of 5, and recess volume ratio of 0.2. The controlling curve will be the lowest; this will give the maximum value of $\overline{M}$ at which the bearing will be stable. Therefore, in using the analysis to determine stability, one must use some caution to be certain the smallest value of $\overline{M}_n$ has been found.

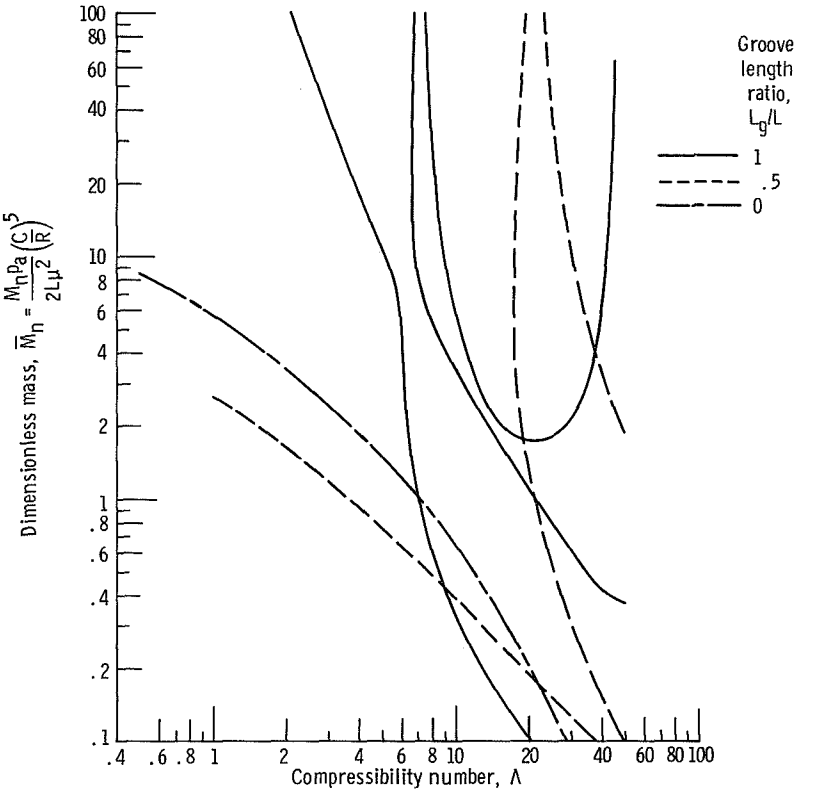

Figure 12. - Multibranch curves. Pressure ratio, 2; feeding parameter, 2; orifice recess volume ratio, 0.2; length to diameter ratio, 1; orifice location parameter L_f/L, 1; groove angle, 30°; groove width fraction, 0.5; groove to land clearance ratio, 2.1.

SUMMARY OF RESULTS

A small eccentricity analysis was performed to determine the steady-state and stability characteristics of externally pressurized bearings with herringbone grooves. Compressibility numbers from 0 to 50 were investigated. The following results were obtained for a bearing with a single row of orifices and a length to diameter ratio of 1:

1. The addition of herringbone grooves to an externally pressurized bearing increases the stability of the bearing. Grooving reduces load capacity at low compressibility numbers but increases load capacity at high compressibility numbers.

2. The fully grooved bearing is generally more stable than the partially grooved bearing. This is especially true at high compressibility numbers. However, the partially grooved bearing has a higher load capacity.

3. At low compressibility numbers, stability increases with increasing supply pressure and feeding parameter. At high compressibility numbers, there is no clear relation of stability with feeding parameter and supply pressure.

4. Load capacity and stability decrease, and the attitude angle increases near the speed where the pressure due to the herringbone groove pumping equals the external supply pressure. This at least partly due to assumptions in the analysis.

5. Orifice recesses decrease stability. The effect is marked at high compressibility numbers. When there are orifice recesses, more than one neutral stability condition can exist at high compressibility numbers. The controlling condition is that which gives the lowest dimensionless mass for neutral stability.

Lewis Research Center,
National Aeronautics and Space Administration,
Cleveland, Ohio, March 30, 1970,
129-03.

APPENDIX A

SYMBOLS

a	orifice radius
C	ridge clearance at zero eccentricity
$\mathscr{C}$	coefficient (see appendix B)
D	bearing diameter
d	orifice recess diameter
e	journal eccentricity
F	bearing load component
f	dimensionless load component, $F/\epsilon p_a LD$
G	dimensionless complex function of ζ
H	ratio of ridge clearance to groove clearance when bearing is concentric, $(h_g/h_r)_o$
h_g	local film thickness over groove, $C(H + \epsilon \cos \theta^*)$
h_r	local film thickness over ridge, $C(1 + \epsilon \cos \theta^*)$
$\mathscr{Im}$	imaginary part of expression
i	$\sqrt{-1}$
k	specific heat ratio
L	bearing length
L_f	length of bearing outboard of orifices
L_g	total axial length of grooves
M	rotor mass per bearing
$\mathscr{M}$	lubricant flow per unit length
$\overline{M}$	dimensionless rotor mass, $(MP_a/2L\mu^2)(C/R)^5$
$\overline{M}_2$	dimensionless rotor mass, $MC\omega^2/p_a LD$
m	dimensionless lubricant flow rate, $4\mathscr{M}_z R\sqrt{\mathscr{R}T}\sqrt{1+\delta^2}/Na^2p_a$
N	number of orifices per bearing
P	dimensionless pressure, p/p_a
p	pressure
p_a	atmospheric pressure
R	bearing radius
$\mathscr{R}$	gas constant
$\mathscr{Re}$	real part of expression
T	absolute temperature
t	time
U_g	surface speed of grooved member
U_p	surface speed of smooth member
V	orifice recess volume
v	orifice recess volume ratio, $NV/\pi DLC$
W	total bearing load
$\overline{W}$	dimensionless load, $W/\epsilon p_a LD$
z	axial coordinate measured from end of bearing
z_f	distance from end of bearing to first row of orifices
z_g	$L_g/2$

α ratio of groove width to width of groove-ridge pair

α_d orifice discharge coefficient

β groove angle (fig. 1)

δ inherent compensation factor, a^2/dC

ϵ eccentricity ratio, e/C

ζ dimensionless axial coordinate, z/L

ζ_f z_f/L

ζ_g z_g/L

θ angular coordinate

θ^* rotating angular coordinate, $\theta - \omega_p t$

Λ bearing compressibility number, $6\mu\omega R^2/p_a C^2$

Λ_s $\Lambda(L/R)$ if smooth member is rotating; $-\Lambda(L/R)$ if grooved member is rotating

Λ_t feeding parameter, $6\mu N_a^2 \sqrt{\mathscr{R}T} \Big/ p_a C^3 \sqrt{1 + \delta^2}$

μ lubricant dynamic viscosity

ρ local lubricant density

σ frequency number, $12\mu\omega_p R^2/p_a C^2$

φ attitude angle

ψ_0 $-(\Lambda_t/2P_{0c})\left[\partial m/\partial(P_c/P_s)\right]\Big|_{\epsilon=0}$

ψ_1 $NV/\pi D^2 C P_{0c}$

ω rotational speed

ω_p whirl frequency

Subscripts:

c condition immediately downstream of orifice

g groove region

n condition at which $f_t = 0$

r radial; ridge region

s condition upstream of orifice

t tangential

z axial direction

θ circumferential direction

0 zero eccentricity

1 perturbed quantity

Superscripts:

+ value of coordinate infinitesimally greater than base value

- value of coordinate infinitesimally less than base value

APPENDIX B

EXPRESSIONS FOR BEARING MASS FLOW AND DIFFERENTIAL EQUATION COEFFICIENTS

Mass Flow Expressions Used in Equation (2) (from ref. 1)

$$\mathscr{M}_{zg} = -\frac{\rho}{12\mu}\frac{h_g^3}{\alpha h_r^3 + (1-\alpha)h_g^3}\left\{(1-\alpha)\left(h_g^3 - h_r^3\right)\sin\beta\cos\beta\frac{1}{R}\frac{\partial p}{\partial\theta}\right.$$

$$\left. + \left[h_r^3 + (1-\alpha)\left(h_g^3 - h_r^3\right)\sin^2\beta\right]\frac{\partial p}{\partial z} - 6\mu(1-\alpha)(U_p - U_g)(h_g - h_r)\sin\beta\cos\beta\right\}$$

$$\mathscr{M}_{zr} = -\frac{\rho}{12\mu}\frac{h_r^3}{\alpha h_r^3 + (1-\alpha)h_g^3}\left\{-\alpha\left(h_g^3 - h_r^3\right)\sin\beta\cos\beta\frac{1}{R}\frac{\partial p}{\partial\theta}\right.$$

$$\left. + \left[h_g^3 - \alpha\left(h_g^3 - h_r^3\right)\sin^2\beta\right]\frac{\partial p}{\partial z} + 6\mu\alpha(U_p - U_g)(h_g - h_r)\sin\beta\cos\beta\right\}$$

$$\mathscr{M}_{\theta r} = -\frac{\rho}{12\mu}\frac{h_r^3}{\alpha h_r^3 + (1-\alpha)h_g^3}\left\{\left[h_g^3 - \alpha\left(h_g^3 - h_r^3\right)\cos^2\beta\right]\frac{1}{R}\frac{\partial p}{\partial\theta}\right.$$

$$\left. - \alpha\left(h_g^3 - h_r^3\right)\sin\beta\cos\beta\frac{\partial p}{\partial z} - 6\mu\alpha(U_p - U_g)(h_g - h_r)\sin^2\beta\right\} + \frac{\rho h_r}{2}(U_p + U_g)$$

Differential Equation Coefficients

$$\mathscr{C}_1 = \frac{H^3 + \alpha(1-\alpha)\left(H^3 - 1\right)^2\sin^2\beta}{\alpha + (1-\alpha)H^3}\frac{R}{L}$$

$$\mathscr{C}_p = \frac{\alpha(1-\alpha)(H^3-1)(H-1)\sin\beta\cos\beta\,\Lambda_s}{H^3+\alpha(1-\alpha)\left(H^3-1\right)^2\sin^2\beta}$$

$$\mathscr{C}_3 = \frac{2\alpha(1-\alpha)\left(H^3-1\right)^2\sin\beta\cos\beta}{H^3+\alpha(1-\alpha)\left(H^3-1\right)^2\sin^2\beta}\frac{L}{R}$$

$$\mathscr{C}_{4a} = \mathscr{C}_3$$

$$\mathscr{C}_{4b} = -\frac{(\alpha H+1-\alpha)\left[\alpha+(1-\alpha)H^3\right]}{H^3+\alpha(1-\alpha)\left(H^3-1\right)^2\sin^2\beta}\left(\frac{L}{R}\right)^2$$

$$\mathscr{C}_{4c} = \frac{\alpha(1-\alpha)(H^3-1)(H-1)\Lambda_s\sin^2\beta}{H^3+\alpha(1-\alpha)\left(H^3-1\right)^2\sin^2\beta}\frac{L}{R}$$

$$\mathscr{C}_5 = \frac{H^3+\alpha(1-\alpha)\left(H^3-1\right)^2\cos^2\beta}{H^3+\alpha(1-\alpha)\left(H^3-1\right)^2\sin^2\beta}\left(\frac{L}{R}\right)^2$$

$$\mathscr{C}_{6a} = \frac{3\alpha(1-\alpha)(H^3-1)(H-1)\sin\beta\cos\beta\left[\alpha(H^2-H-1)-(1-\alpha)H^2(H^2+H-1)\right]}{\left[H^3+\alpha(1-\alpha)\left(H^3-1\right)^2\sin^2\beta\right]\left[\alpha+(1-\alpha)H^3\right]}\frac{L}{R}$$

$$\mathscr{C}_{6b} = \frac{\left[\alpha+(1-\alpha)H^3\right]}{H^3+\alpha(1-\alpha)\left(H^3-1\right)^2\sin^2\beta}\left(\frac{L}{R}\right)^2$$

$$\mathscr{C}_{6c} = \frac{3\alpha(1-\alpha)(H-1)^2H^2\Lambda_s\sin^2\beta}{\left[H^3+\alpha(1-\alpha)\left(H^3-1\right)^2\sin^2\beta\right]\left[\alpha+(1-\alpha)H^3\right]}\frac{L}{R}$$

$$\mathscr{C}_7 = \frac{3\alpha(1-\alpha)(H-1)(H^2-1)\Lambda_s\sin\beta\cos\beta\left[H^2(H^2+1)+\alpha(1-\alpha)\left(H^3-1\right)^2\sin^2\beta\right]}{\left[H^3+\alpha(1-\alpha)\left(H^3-1\right)^2\sin^2\beta\right]^2}$$

$$\mathscr{C}_m = \frac{3\alpha H^2 (H - 1)\left\{1 + (1 - \alpha)(H^3 - 1)\left[2 + (1 - \alpha)(H^3 - 1)\right] \sin^2 \beta\right\}}{\left[H^3 + \alpha(1 - \alpha)\left(H^3 - 1\right)^2 \sin^2 \beta\right]^2}$$

In the ungrooved portion of the bearing, these coefficients become

$$\mathscr{C}_p = 0$$

$$\mathscr{C}_3 = 0$$

$$\mathscr{C}_{4a} = 0$$

$$\mathscr{C}_{4b} = -\left(\frac{L}{R}\right)^2$$

$$\mathscr{C}_{4c} = 0$$

$$\mathscr{C}_5 = \left(\frac{L}{R}\right)^2$$

$$\mathscr{C}_{6a} = 0$$

$$\mathscr{C}_{6b} = \left(\frac{L}{R}\right)^2$$

$$\mathscr{C}_{6c} = 0$$

$$\mathscr{C}_7 = 0$$

APPENDIX C

COMPUTER PROGRAM FOR ANALYSIS OF EXTERNALLY PRESSURIZED HERRINGBONE GROOVED GAS-LUBRICATED JOURNAL BEARING

The program for determining steady-state and stability characteristics of the externally pressurized herringbone bearing is written in FORTRAN IV, version 13, for use on the IBM 7094-II digital computer at Lewis Research Center. Minor modifications may be necessary to allow the program to be used with other computing systems.

Program Input

Two variables are set within the program: k, the specific heat ratio of the lubricant gas, and RKEP, an accuracy parameter. As the program operates, the step size in the Runge-Kutta differential equation solver is successively halved until the magnitude of the bearing load W varies by less than RKEP times W.

The remainder of the information needed by the program is read from punched cards. A triad of cards shows each configuration to be analyzed. The first gives geometric and operating parameters; the second contains the array of bearing numbers Λ to be used (up to 19 values); and the third gives initial estimates of the frequency number σ, one for each Λ value. Specific formats follow.

Geometric configuration card: Format (13F6.0). - Succeeding eight-column fields contain, in real format (with decimal point): β, α, H, L/D, L_g/L, SGN, L_f/L, Λ_t, P_s, v, α_d, and $1 + \delta^2$. SGN is +1.0 if the smooth member of the bearing is rotating, and -1.0 if the grooved member is rotating.

Bearing number array card: Format (I4, 19F4.1). - First four-column field: the number of Λ's in the array, integer format, right adjusted. Succeeding four-column fields: the values of Λ for which calculations are desired, real format (with decimal point). Positive Λ means the program will search for a root of $f_t = 0$ such that $\partial f_t / \partial \sigma < 0$. The reverse is true if Λ is negative.

Frequency number estimate card: Format (4X, 19F4.0). - First four-column field is not read. Succeeding four-column fields contain, in real format (with decimal point), the initial estimate of frequency number σ, one value for each Λ.

Any number of geometric configurations may be examined in one run of the program. Sample program input on a FORTRAN coding sheet appears as figure 13.

The first card is a geometric configuration card which indicates that $\beta = 30^o$, $\alpha = 0.5$, H = 2.1, L/D = 1, $L_g/L = 1$, SGN = -1, $L_f/L = 1$, $\Lambda_t = 2$, $P_s = 2$, v = 0, $\alpha_d = 0$, and $1 + \delta^2 = 1$. The second card, the Λ array, indicates there are 13 Λ values ranging

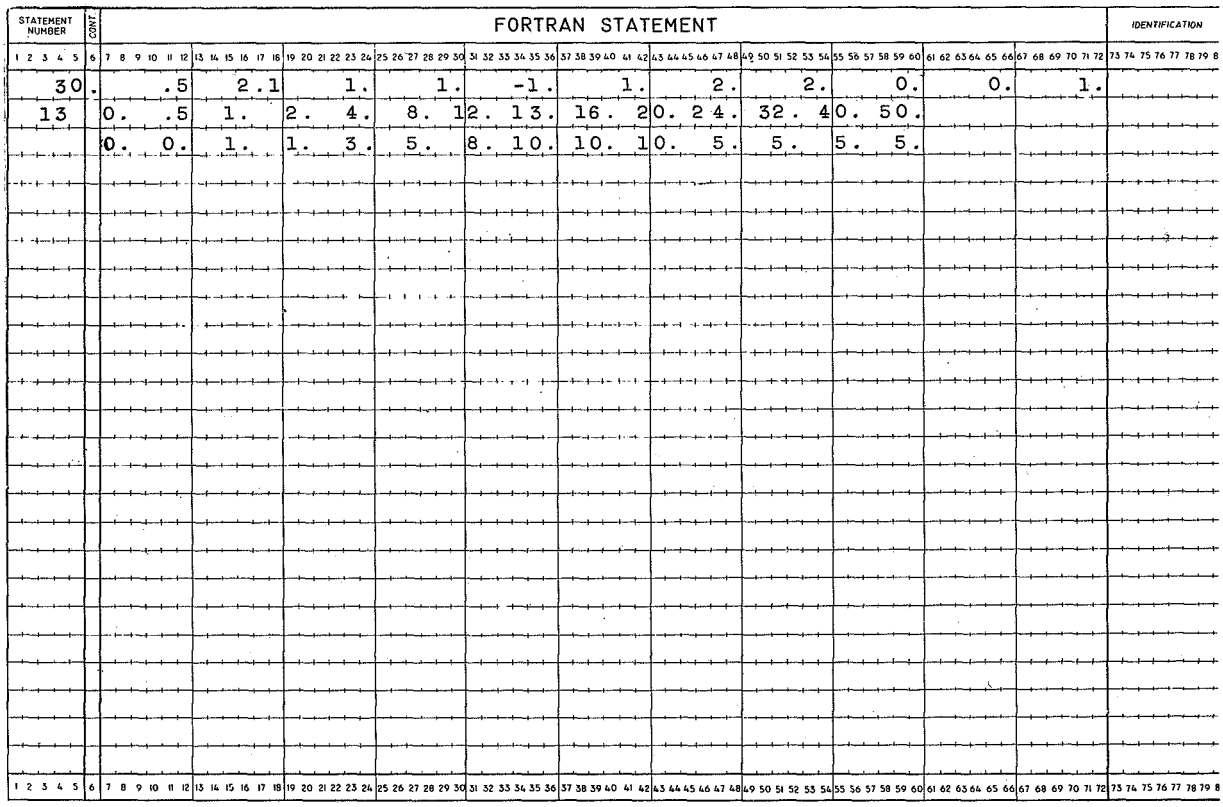

Figure 13. - Sample program input.

from 0 to 50. The third card is the σ estimate card, showing initial estimates of σ, which correspond to the Λ array. Any number of these sets of three cards may be used.

When the orifice discharge coefficient is specified as zero on the geometric configuration card, the actual value used is computed as a function of the pressure ratio across the orifice, using the information in reference 2. If a nonzero α_d is specified, that value is used.

Program Output

Output consists of two sheets for each configuration: A working sheet and a calculation summary sheet.

The working sheet shows the geometric and operating parameters, trial values for determination of the pressure downstream of the orifices, final value of orifice downstream pressure, ψ_0, ψ_1, and RKEP. For each Λ in the array and for each trial value of σ there appear Λ, f_r, f_t, $W/(\epsilon p_a LD)$, φ, $\overline{M}_2$, final Runge-Kutta step size, $\overline{M}$, ω_p/ω, σ, and a coefficient applied to ψ_o in equation (24). This coefficient, in refer-

ence 4, was taken as 1 when σ was 0, and 0 otherwise. In the present work it is always 1. A sample working sheet appears as figure 14. The data appearing thereon were generated from the values shown in the sample input.

```
          EXTERNALLY PRESSURIZED HERRINGBONE BEARING -- GROOVED MEMBER ROTATING

 BETA      ALFA       H         L/D       L(G)/L     L(O)/L    LAMBDA T    PS/PA       VC       CRF.COEF     1+D**2     K=CP/CV
 30.00     0.500      2.100     1.000      1.000      1.000      2.000      2.000       0        VARIABLE      1.000      1.400

 SOLUTION FOR POC        LAMBDA= 0
      1    PC  1.4142136     PC1  1.3121654     MO -0.8383     MAXMO  0            UNCHOKED   ORIF COEF 0.661
      2    PC  1.3631895     PC1  1.3026086     MO -0.8687     MAXMO  0            UNCHOKED   ORIF COEF 0.670
      3    PC  1.3026086     PC1  1.2983005     MO -0.9015     MAXMO  0            UNCHOKED   ORIF COEF 0.682
      4    PC  1.2983005     PC1  1.2982814     MO -0.9037     MAXMO  0            UNCHOKED   ORIF COEF 0.682

   PC 1.298     PC/PS 0.649        PSO-0.783        PS1 0            RKDX REDUCED UNTIL ERROR .LE. 0.500E-02

 LAMBDA    FR/EPALD    FT/EPALD     W/EPALD      PHI     MCW2/PALD       RKDX      MPC5/2LR5MU2 WHIRL RATIO VIB NR SIGMA  PSC COEF
 0          0.282      -0.701E-C2   0.2819     -1.425       0           0.1250        0            10CC.0       C           1.CCCC
 0          0.291       0.775E-C1   0.3012      14.90       0           0.1250       41.916        1CCC.0      -1.CCCC      1.CCCC
 0          0.282       0.919E-C4   0.2818      0.187E-01   0           0.1250       5891.0        10C0.0      -0.8300E-01  1.CCCC


 SOLUTION FOR POC        LAMBDA= 0.500
      1    PC  1.4142136     PC1  1.3337132     MO -0.8383     MAXMO  0.9587E-01   UNCHOKED   ORIF COEF 0.661
      2    PC  1.3739634     PC1  1.3285685     MO -0.8625     MAXMO  0.9587E-01   UNCHOKED   ORIF COEF 0.668
      3    PC  1.3285685     PC1  1.3264548     MO -0.8878     MAXMO  0.9587E-01   UNCHOKED   ORIF COEF 0.677
      4    PC  1.3264548     PC1  1.3264503     MO -0.8890     MAXMO  0.9587E-01   UNCHOKED   ORIF COEF 0.677

   PC 1.326     PC/PS 0.663        PSO-0.807        PS1 0            RKDX REDUCED UNTIL ERROR .LE. 0.500E-02

 LAMBDA    FR/EPALD    FT/EPALD     W/EPALD      PHI     MCW2/PALD       RKDX      MPC5/2LR5MU2 WHIRL RATIO VIB NR SIGMA  PSC COEF
 0.5CC      0.313       0.271E-C1   C.3137      4.959       0           0.1250        0            0            0           1.0000
 0.5CC      0.311       0.106E-C1   C.3114      1.956       7.7793      0.1250        1120.2       0.2000       C.2C00      1.CCCC
 0.500      0.311      -0.594E-C2   C.3106     -1.096       1.9410      0.1250        279.51       0.4000       0.4C00      1.0000
 0.500      0.311       0.581E-05   0.3107      0.107E-02   2.8828      0.1250        415.12       0.3283       C.3283      1.CCCC


 SOLUTION FOR POC        LAMBDA= 1.000
      1    PC  1.4142136     PC1  1.3576819     MO -0.8383     MAXMO  0.1917       UNCHOKED   ORIF COEF 0.661
      2    PC  1.3859477     PC1  1.3554464     MO -0.8554     MAXMO  0.1917       UNCHOKED   ORIF COEF 0.666
      3    PC  1.3554464     PC1  1.3545969     MO -0.8731     MAXMO  0.1917       UNCHOKED   ORIF COEF 0.672
      4    PC  1.3545969     PC1  1.3545963     MO -0.8735     MAXMO  0.1917       UNCHOKED   ORIF COEF 0.672

   PC 1.355     PC/PS 0.677        PSO-0.830        PS1 0            RKDX REDUCED UNTIL ERROR .LE. 0.500E-02

 LAMBDA    FR/EPALD    FT/EPALD     W/EPALD      PHI     MCW2/PALD       RKDX      MPC5/2LR5MU2 WHIRL RATIO VIB NR SIGMA  PSC COEF
 1.000      0.347       0.575E-01   0.3513      9.414       0           0.1250        0            0            0           1.CCCC
 1.000      0.339      -0.22CE-C1   0.3394     -3.718       1.3547      0.1250        48.769       0.5000       1.0CC0      1.CCCC
 1.000      0.34C       0.101E-C1   C.3398      1.708       3.7743      0.1250        135.87       0.3000       C.6C00      1.CCCC
 1.000      0.339       0.252E-C4   0.3391      0.426E-02   2.5726      0.1250        92.613       0.3630       0.7261      1.CCCC


 SOLUTION FOR POC        LAMBDA= 2.000
      1    PC  1.4142136     PC1  1.4108198     MO -0.8383     MAXMO  0.3835       UNCHOKED   ORIF COEF 0.661
      2    PC  1.4125167     PC1  1.4108133     MO -0.8394     MAXMO  0.3835       UNCHOKED   ORIF COEF 0.661
      3    PC  1.4108133     PC1  1.4108112     MO -0.8404     MAXMO  0.3835       UNCHOKED   ORIF COEF 0.662

   PC 1.411     PC/PS 0.705        PSO-0.874        PS1 0            RKDX REDUCED UNTIL ERROR .LE. 0.500E-02
```

Figure 14. - Example of working sheet.

The calculation summary sheet again shows the geometric and operating parameters, and, for each Λ of the Λ array, $W/(\epsilon p_a LD)$, φ, ω_p/ω, σ_n, $\overline{M}_{2n}$, $\overline{M}_n$, P_{0c}, $(\partial f_t/\partial\sigma)_n$, m_0, α_d (actual value used), and the ψ_0 coefficient. Figure 15 shows an example of a summary sheet. Again, the data correspond to those of the sample input. Program execution time for the sample input was 20 seconds.

EXTERNALLY PRESSURIZED HERRINGBONE BEARING -- GROOVED MEMBER ROTATING

L/D	LO/L	LAMBDA T	1+DELTA**2	K=CP/CV	ORIF COEF	REC.VOL.VC
1.000	1.000	2.000	1.000	1.400	VARIABLE	0

PS/PA	BETA	ALFA	H	LG/L	RKEP
2.000	30.00	0.500	2.100	1.000	0.500E-02

BRG NR LAMBDA	BRG LOAD W/EPALO	ATT ANGLE PHI	WHIRL RATIO WP/OMEGA	VIB NR SIGMA	STABILITY PARAMETERS MCW2/PALO	MPC5/2LR5MU2	PC/PA	D(FT) D(SIGMA)	MASS FLOW MO	ORIFICE COEF AO	PSO COEF
0	0.282	-1.425	1000.	-0.830E-01	0	0.589E 04	1.298	-0.84E-01	-0.904	C.682	1.000
0.500	0.314	4.959	0.328	0.328	2.883	415.1	1.326	-0.83E-01	-0.889	C.677	1.000
1.000	0.351	9.414	0.363	0.726	2.573	92.61	1.355	-0.80E-01	-0.874	C.672	1.000
2.000	0.434	14.10	0.371	1.484	2.863	25.77	1.411	-0.76E-01	-0.840	C.662	1.000
4.000	0.592	15.29	0.355	2.840	3.948	8.884	1.523	-0.66E-01	-0.765	C.642	1.000
8.000	0.815	11.55	0.313	5.005	6.796	3.823	1.743	-0.56E-01	-0.572	C.608	1.000
12.00	0.920	13.33	0.340	8.162	5.828	1.457	1.945	-0.47E-01	-0.271	C.584	1.000
13.00	0.896	20.24	0.397	10.32	3.318	0.707	1.984	-0.57E-01	-0.146	C.581	1.000
16.00	1.022	9.870	0.306	9.778	8.340	1.173	2.079	-0.37E-01	0.329	C.586	1.000
20.00	1.138	4.334	0.183	7.303	30.48	2.743	2.294	-0.18E-01	0.655	C.608	1.000
24.00	1.238	2.377	0.111	5.314	95.01	5.938	2.533	-0.12E-01	0.915	C.632	1.000
32.00	1.432	0.822	0.411E-01	2.631	829.1	29.15	3.042	-0.86E-02	1.361	C.679	1.000
40.00	1.629	0.411	0.212E-01	1.699	0.357E 04	80.33	3.575	-0.72E-02	1.750	C.716	1.000

Figure 15. - Calculation summary sheet.

```
$IBFTC EPHB

C  SMALL ECCENTRICITY STABILITY ANALYSIS FOR HERRINGBONE BEARING WITH ORIFICES
       DIMENSION SLAM(20),SW(20),SPHI(20),SW3(20),SCM(20),SSIG(20)
       DIMENSION ACM(20),SD(20),SPC(20),SMU(20),SAO(20),SPS(20)
       COMMON /CY4/ DP,DC,DG,DGP
       COMMON /CFM/ PCR,K,SK1,SK2,VARA,AO
       COMMON /CHK/ CC,UC,C
       COMMON /CFF/ HLM,CP,C2A,C2B,IC3A,IC4A,IC4W,ICS4W,IC6A,IC6W,ICS6W,
      1 C5A,C7A,C8B,HLM2,CS5
       COMMON /CHS/ LAMBDA,PSO,PSI,CMA,CMC,W,PHI,WR,RKEP,Q,L,PC,C4B,C4C,
      1  C6B,C6C,FIRST,SIZ,CPS
       COMMON /CHR/ CG,QD,ZG,ZO
       REAL L,LG,LO,LT,MU,C(2),K,LS,LAMBDA
       COMPLEX IC3A,IC4A,IC4W,ICS4W,IC6A,IC6W,ICS6W
       COMPLEX Y(2),A(2),B(2),XF,CDX,CG,DG
       LOGICAL VARA,FIRST
       EXTERNAL F1
       ALPHA(P) = .84276 +  (.06451 + (-.76195 + .43415*P)*P)*P
       EPS = 1.E-4
       EPSW = 1.E-3
       K = 1.4
       SK1 = SQRT (2.*K/(K+1.))*(2./(K+1.))**(1./(K-1.))
       SK2 = SQRT (2.*K/(K-1.))
       PCR = (2./(K+1.))**(K/(K-1.))
       RKEP = .005
3      READ (5,5) BETAD,ALFA,H,CL,LG,SGN,LO,LT,PS,VC,AO,D1
5      FORMAT (13F6.0)
C   BETAD = GROOVE ANGLE, DEGREES. ALFA = GROOVE WIDTH FRACTION. H = GROOVE
C   CLEARANCE/LAND CLEARANCE, CL = L/D. LG = GROOVE LENGTH FRACTION LG/L
C  SGN = +1.0 FOR SMOOTH MEMBER ROTATING, -1.0 FOR GROOVED MEMBER ROTATING
C  LO=FRACTION OF LENGTH OUTBOARD OF ORIFICES, LT=LAMBDA(T), PS=PRESSURE RATIO
C  VC=ORIFICE RECESS VOLUME RATIO, AO=ORIFICE COEFFICIENT, D1=1+DELTA**2
C  LG=1 DENOTES FULLY GROOVED BEARING, LO=1 DENOTES SINGLE ROW OF ORIFICES
       IF (LG.EQ.0.) SGN = 0.
       VARA = .FALSE.
       IF (AO.EQ.0.) VARA = .TRUE.
       READ (5,1) IS, (SLAM(I), I = 1, IS)
1      FORMAT (I4, 19F4.1)
       READ (5,2) (SSIG(I), I = 1, IS)
2      FORMAT (4X,19F4.0)
4      FORMAT (1H1/8X,65HSMALL ECCENTRICITY ANALYSIS FOR HERRINGBONE BEAR
      1ING WITH ORIFICES )
       PCA = PS*PCR
       BETA = SIGN (BETAD/57.2957796, SGN)
       L = 2.*CL
       SI= SIN(BETA)
       CO= COS(BETA)
       ALFI= 1.-ALFA
       H2= H*H
       H3= H2*H
       DN= ALFA+ALFI*H3
       H32= (H3-1.)**2
       AA= ALFA*ALFI
       AS= AA*SI*SI
       ASC= AA*SI*CO
       D2= H3+AS*H32
       H31= (H3-1.)*(H-1.)
       C1= D2/(DN*L)
       WRITE (6,707)
```

```
707   FORMAT (1H1/15X,45HEXTERNALLY PRESSURIZED HERRINGBONE BEARING -- )
      IF (SGN) 9, 90, 91
91    WRITE (6,808)
808   FORMAT (1H+ 60X, 22HSMOOTH MEMBER ROTATING )
      GO TO 902
90    WRITE (6,890)
890   FORMAT (1H+ 60X,17HUNGROOVED BEARING )
      GO TO 902
9     WRITE (6,909)
909   FORMAT (1H+ 60X, 23HGROOVED MEMBER ROTATING )
902   WRITE (6,6)
6     FORMAT (6HL BETA 7X,4HALFA 8X,1HH 9X,3HL/D 7X,6HL(G)/L 5X,6HL(O)/_
     1 4X,8HLAMBDA T 4X,5HPS/PA 8X,2HVC 6X,8HORF.COEF 4X,6H1+D**2 5X,
     2 7HK=CP/CV )
      IF (.NOT.VARA) WRITE (6,61) BETAD,ALFA,H,CL,LG,LO,LT,PS,VC,AO,D1,<
61    FORMAT (12G11.3)
      IF (VARA)      WRITE (6,62) BETAD,ALFA,H,CL,LG,LO,LT,PS,VC,   D1,<
62    FORMAT (9G11.3,8HVARIABLE 3X 2G11.3)
      ZG = LG/2.
      ZO = LO/2.
      C2A = 2.
      IC3A = (0.,2.)*ASC*H32/D2*L
      IC4A = IC3A
      C5A = (H3 + AA*CO*CO*H32)/D2*L*L
      IC6A = (0.,3.)*ASC*H31*(ALFA*(H2-1.)-ALFI*H2*(H2+H-1.))/D2/DN*L
      C6B = L/C1
      C4B = -C6B*(ALFI + ALFA*H)
      CS5 = L*L
      DPT = 3./DN/D2*ALFA*H2*(H-1.)*(1.+ALFI*(H3-1.)*SI*SI*(2.*ALFA
     1 + ALFI*(H3+1.)))
      DG = IC3A*C1*L/2.
      DGP = C1*L
      DO 300 I=1,IS
      SDS = SIGN (1., SLAM(I))
      SLAM(I) = ABS (SLAM(I))
      LAMBDA = SLAM(I)
      IF (LAMBDA.EQ.0..AND.(PS.EQ.1..OR.LT.EQ.0.)) GO TO 300
      IF (LAMBDA.EQ.0..AND.(PS.EQ.1..OR.LT.EQ.0.)) GO TO 300
      IF (LG.EQ.0..AND.I.GT.1) GO TO 27
      LS = SGN*L*LAMBDA
      CP = ASC*H31*LS/D2
      WRITE (6,8)  LAMBDA
8     FORMAT (17HLSOLUTION FOR POC 8X 7HLAMBDA= G11.3/)
      HLM = 0.
      HLM2 = 0.
      MO = 0.
      PC = 1. + CP*ZG
      IF (LT.EQ.0.) GO TO 25
      PC = AMAX1 (PC, SQRT(PS))
      XF = ZG
      CDX = LG/32.
      DO 20 J = 1, 10
      IF (.NOT. VARA) GO TO 15
      P = PC/PS
      IF (P.GT.1.) P = 1./P
      AO = ALPHA(P)
15    MO = FMU (PC,PS,DMO)*AO
      DMO = AO*DMO
      DMP = DMO/PS
      UMO = 2.*C1*CP/LT
```

```
      HLM = LT*AMIN1(MO,UMO)/2.
      HLM2 = HLM*L
      HL4 = HLM/C1
      IF (MO.GE.UMO) GO TO 81
      IF (CP.EQ.0.) GO TO 22
      POG = SQRT(AMAX1(PC*PC + L*LT*MO*(ZO-ZG) ,0.))
      PL = ALOG ((POG*CP-HLM)/(CP-HLM))
      ZG1 = (POG-1. + HLM/CP*PL)/CP
      POG = POG*CP
      DZG = (PC + CL*LT*(ZO-ZG)*DMP)/(POG-HLM) + LT/(2.*C1*CP*CP)*DMP
     1  *(PL + HLM*(POG-CP)/(POG-HLM)/(CP-HLM))
      PC1 = PC - (ZG1-ZG)/DZG
      GO TO 24
22    IF (ZG.EQ.0.) GO TO 23
      PG2 = PC*PC + L*LT*MO*(ZO-ZG)
      PC1 = PC - (HLM*ZG-.5+.5*PG2)/(PC+.5*(1.-PC*PC)/MO*DMP)
      GO TO 24
23    ZG1 = ZO - (1.-PC*PC)/HLM2/2.
      DZG = PC/HLM2 + (ZO-ZG1)/MO*DMP
      PC1 = PC - ZG1/DZG
      IF (PC.LT.PCA.AND.PC1.LT.PCA) PC1=SQRT(1.-2.*HLM2*ZO)
      GO TO 24
81    Y(2) = 1.
      IF (LG.EQ.0.) GO TO 92
      Y(1) = 0.
      CALL RKGS (F1,Y,XF,DX,A,B,2)
92    PC1 = SQRT(AMAX1(REAL(Y(2))**2 - L*LT*AMIN1(MO,JMO)*(ZO-ZG),0.))
24    WRITE (6,10) J,PC,PC1,MO,UMO,C,AO
10    FORMAT (I8,4X 2HPC G15.7,3HPC1 G15.7,2HMOG12.4,5HMAXMOG12.4,A4,A6,
     1  3X 9HORIF COEF G10.3)
      IF (ABS(PC1/PC - 1.).LE.EPS) GO TO 25
      IF (PC.LT.PCA.AND.PC1.LT.PCA) PC=PC1
      IF (MO.LT.UMO.AND.J.GT.1) PC = PC1
20    PC = (PC+PC1)/2.
      SW(I) = 0.
      GO TO 300
25    PSO = -LT/2.*DMO/PC
      PS1= VC*CL/PC
      PCS = PC/PS
      Q=L*MO*LT/PC
      QD = Q*(D1 + .5)/D1
      Q = Q/PC/2.
      WRITE (6,26) PC,PCS,PSO,PS1,RKEP
26    FORMAT (6HK    PC G10.3,5HPC/PS G10.3,6H   PSO G10.3,6H   PS1
     1 G10.3,32H   RKDX REDUCED UNTIL ERROR .LE. G10.3)
      PSO = L*PSO/PS
      PS1 = L*PS1
27    SPC(I) = PC
      SMO(I) = MO
      SAO(I) = AO
      SIG1 = SSIG(I)
      DS = 1.
      IF (LAMBDA.NE.0.) DS = .4*LAMBDA
      C2B = -CP
      C4C = AS*H31*LS*L/D2
      C6C = 3.*AS*(H-1.)**2*H2*LS/D2/DN*L
      C7A = 3.*ASC*(H-1.)*(H2-1.)*LS*(H2*(H2+1.)+AS*H32)/D2/D2
      C8B = CP
      DP = DPT*HLM2
      DC = C7A*C1*L
```

```
      WRITE (6,140)
140   FORMAT (8HK LAMBDA 4X,8HFR/EPALD 3X,8HFT/EPALD 4X,7HW/EPALD 2X,
     1 4X 3HPHI 4X 9HMOW2/PALD 7X 4HRKDX 5X 12HMPC5/2LR5MJ2 1X
     2 11HWHIRL RATIO 1X 12HVIB NR SIGMA 2X 8HPSO COEF )
      FIRST = .TRUE.
      CALL HYST (0.,GIO)
      FIRST = .FALSE.
      IF (LAMBDA.EQ.0.) GIO=.25
      SW(I) = W
      SPHI(I) =PHI
      CALL HYST (SIG1, GI1)
      SIG = SIG1
      IF (ABS(GI1/GIO).LE.EPSW) GO TO 299
      DS1 = SDS*SIGN (DS, GI1)
      SIG2 = SIG1
      DO 150 J = 1, 20
      SIG2 = SIG2 + DS1
      CALL HYST (SIG2, GI2)
      SIG = SIG2
      IF (ABS(GI2/GIO).LE.EPSW) GO TO 299
      DS2 = SDS*SIGN (DS, GI2)
      IF (DS2 - DS1) 220, 210, 220
210   SIG1 = SIG2
150   GI1 = GI2
      GO TO 299
220   DO 235 J = 1, 10
      SIG = (GI2*SIG1 - GI1*SIG2)/(GI2 - GI1)
      SD(I) = (GI2 - GI1)/(SIG2 - SIG1)
      CALL HYST (SIG, GI)
      IF(ABS(GI/GIO).LE.EPSW) GO TO 299
      IF (ABS(GI2).GT.ABS(GI1)) GO TO 230
      GI1 = GI2
      SIG1 = SIG2
230   GI2 = GI
235   SIG2 = SIG
299   SW3(I)=WR
      ACM(I) = CMA
      SCM(I)=CMC
      SSIG(I) = SIG
      SPS(I) = CPS
300   CONTINUE
      WRITE (6,707)
      IF (SGN.LT.0.) WRITE (6,909)
      IF (SGN.EQ.0.) WRITE (6,890)
      IF (SGN.GT.0.) WRITE (6,808)
      WRITE (6,600) CL,LO,LT,DI,K
600   FORMAT (1HL 8X,3HL/D 8X,4HLO/L 6X,8HLAMBDA T 4X,10H1+DELTA**2 3X,
     1 7HK=CP/CV 4X,9HORIF COEF 2X,10HREC.VOL.VC /5X,5G12.3)
      IF (.NOT.VARA) WRITE (6,601) AO,VC
601   FORMAT (1H+ 64X 2G12.3)
      IF (VARA) WRITE (6,602) VC
602   FORMAT (1H+ 65X 8HVARIABLE G15.3)
      WRITE (6,603) PS,BETAD,ALFA,H,LG,RKEP
603   FORMAT(/8X 5HPS/PA 7X 4HBETA 8X 4HALFA 11X 1HH 10X 4HLG/L 8X
     1  4HRKEP /5X 7G12.3)
      WRITE (6,325) (SLAM(I),SW(I),SPHI(I),SW3(I),SSIG(I),ACM(I),SCM(I),
     1 SPC(I),SD(I),SMO(I),SAO(I),SPS(I),I = 1, IS)
```

```
325   FORMAT (/1HL  3X,6HBRG NR 3X,8HBRG LOAD 2X,22HATT ANGLE  WHIRL RAT
     1IO 2X,6HVIB NR 3X,20HSTABILITY PARAMETERS 15X 5HD(FT) 6X 4HMASS
     2  4X 7HORIFICE 5X 3HPSO /
     1 4X 6HLAMBDA 4X 7HW/EPALO 5X 3HPHI 6X 8HWP/OMEGA 4X 5HSIGMA 4X
     2 30HMCW2/PALO  MPC5/2LR5MU2  PC/PA 4X 8HD(SIGMA) 3X 7HFLOW MO
     3  2X 7HCOEF AO 5X 4HCOEF /
     4 (/3X 2G10.3,G11.3,G12.3,2G10.3,2G12.3,G9.2,G11.3,G10.3,F5.3))
      GO TO 3
      END
```

```
$IBFTC HYDST

      SUBROUTINE HYST (SIGMA, GI)
      COMMON /COEF/ HLM,CP,C2A,C2B,IC3A,IC4A,IC4W,ICS4W,IC6A,IC6W,ICS6W,
     1 C5A,C7A,C8B,HLM2,CS5
      COMMON /CHS/ LAMBDA,PSO,PSI,CMA,CMC,W,PHI,WR,RKEP,Q,L,PC,C4B,C4C,
     1  C6B,C6C,FIRST,GIZ,CPS
      COMMON /CHR/ CG,QD,ZG,ZO
      REAL LAMBDA,L
      COMPLEX AA,AB,BA,BB,CA,CB,CG,DX
      COMPLEX IC3A,IC4A,IC4W,ICS4W,IC6A,IC6W,ICS6W
      LOGICAL FIRST
      IF (FIRST.OR.SIGMA.NE.0.) GO TO 10
      GI = GIZ
      WR = 1000.
      IF (LAMBDA.NE.0.) WR = 0.
      CMC = 0.
      CMA = 0.
      RETURN
10    CPS = 1.
      CG = PSO*CPS + Q + (0.,1.)*SIGMA*PSI
C  PSO=0 MEANS ORIFICE MASS FLOW DOES NOT VARY WITH THETA
      DX = .25
      DX = 0.
      WR=LAMBDA - SIGMA
      IC4W = (0.,1.)*(C4B*WR + C4C)
      IC6W = (0.,1.)*(C6B*WR + C6C)
      ICS6W = (0.,1.)*CS5*WR
      ICS4W = -ICS6W
      DO 110 N = 1, 8
      BA = 0.
      BB = (-1.,-1.)
      CALL RKLP (BA,DX,AA,CA)
      CALL RKLP (BB,DX,AB,CB)
      CA = -3.14159265*(AB*CA - AA*CB)/(AB - AA)
      IF (CABS(DX/CA-1.) .LE. RKEP) GO TO 120
      DX = .5*DX
```

```
110   TDX = CA
120   RDX=DX
      GR = REAL (CA)
      GI = AIMAG(CA)
      IF (FIRST) GIZ = GI
      W = CABS(CA)
      PHI = ATAN2(GI,GR)*57.2957796
      WR = 1000.
      CMC = 0.
      IF (SIGMA.NE.0.) CMC = 144.*GR/SIGMA**2
      CMA = CMC*LAMBDA**2/36.
      IF (LAMBDA.NE.0.) WR = .5*SIGMA/LAMBDA
      WRITE (6,145) LAMBDA,GR,GI,W,   PHI,CMA,RDX,CMC,WR,SIGMA,CPS
145   FORMAT (3G11.3, G12.4,G11.3,G12.4,2G13.4,3G12.4)
      RETURN
      END
```

```
$IBFTC FM

      FUNCTION FMO  (PC,PS,DMO)
      COMMON /CFM/ PCR,K,SK1,SK2,VARA,AO
      COMMON /CHK/CC,UC,C(2)
      REAL K
      LOGICAL VARA
      DALPH (Y) = .06451 + (-2.*.76195 + 3.*.43415*Y)*Y
      IF (PC.GT.PS) GO TO 20
      PCS = PC/PS
      AD =  DALPH(PCS)
      PM = -PS
      GO TO 30
20    PCS= PS/PC
      AD = -PCS*PCS*DALPH(PCS)
      PM = PC
30    IF (PCS.GT.PCR) GO TO 40
      FMO = PM*SK1
      DMO= 0.
      IF (PC.GT.PS) DMO = PS*SK1
      IF (VARA) DMO = DMO + FMO*AD/AO
      C(1) = CC
      RETURN
40    PK = PCS**(1./K)
      PSQ = SQRT (1.-PCS/PK)
      FMO = PM*SK2*PK*PSQ
      IF (PS.GT.PC) DMO = -PS*SK2*(PK/PCS-(K+1.)/2.)/PSQ/K
      IF (PS.LT.PC) DMO =  PS*SK2*(K-1.)/K*(PK-PCS/2.)/PSQ
      IF (PS.EQ.PC) DMO =  1.E10
      IF (VARA) DMO = DMO + FMO*AD/AO
      C(1)=UC
      RETURN
      END
```

```
$IBFTC BD

      BLOCK DATA
      COMMON /CHK/CC,UC,C(2)
      DATA CC,UC,C(2) / 1H ,4H  UN,6HCHOKED /
      END
```

```
$IBFTC RKLPS

      SUBROUTINE RKLP (GIN,DX,AD,CD)
      COMMON /CY4/ DP,DC,DG,DGP
      COMMON /CHR/ CG,QD,ZG,ZO
      COMPLEX Y(5),A(5),B(5),GIN,AD,CD,CG, XF,CDX
      COMPLEX DG
      EXTERNAL F2,F3,F4
      Y(1)= 0.
      Y(2) = 1.
      Y(3) = 0.
      Y(4) = GIN
      Y(5) = 0.
      IF (ZG.EQ.0.) GO TO 10
      XF = ZG
      CDX = ZG/AMAXO(IFIX(ZG/DX+.1),1)
      CALL RKGC (F2,Y,XF,CDX,A,B,5)
      Y(4) = DP/Y(2) + DC + DG*Y(3) + DGP*Y(4)
10    IF (ZG.EQ.ZO) GO TO 15
      XF = ZO
      CDX = (ZO-ZG)/AMAXO(IFIX((ZO-ZG)/DX+.1),1)
      CALL RKGC (F3,Y,XF,CDX,A,B,5)
15    Y(4) = Y(4) - QD - CG*Y(3)
      IF (ZO.EQ..5) GO TO 20
      XF = .5
      CDX = (.5-ZO)/AMAXO(IFIX((.5-ZO)/DX+.1),1)
      CALL RKGC (F4,Y,XF,CDX,A,B,5)
20    AD = Y(4)
      CD = Y(5)
      RETURN
      END
```

```
$IBFTC FF

      SUBROUTINE F1 (Y,YP)
      COMMON /CFF/ HLM,CP,C2A,C2B,IC3A,IC4A,IC4W,ICS4W,IC6A,IC6W,ICS6W,
     1 C5A,C7A,C8B,HLM2,CS5
      COMPLEX IC3A,IC4A,IC4W,ICS4W,IC6A,IC6W,ICS5W,Y(1),YP(1)
C SUBROUTINE FOR PO
      YP(1)= 1.
      YP(2) = CP- HLM/Y(2)
      RETURN
      ENTRY F2 (Y,YP)
C SUBROUTINE FOR G IN GROOVED REGION
      YP(2) = CP -HLM/Y(2)
      YP(4) = -((C2A*YP(2)+C2B)/Y(2) + IC3A      )*Y(4) - ((
     1  IC4A*YP(2)+IC4W +  (-YP(2)+C8B)*YP(2)/Y(2))/Y(2)-C5A)*Y(3)
     2 + IC6A*YP(2)+IC6W          - C7A*YP(2)/Y(2)
      GO TO 10
      ENTRY F3 (Y,YP)
C SUBROUTINE FOR G IN SMOOTH REGION
      YP(2) = -HLM2/Y(2)
      YP(4) = -C2A*YP(2)*Y(4)/Y(2) - ((ICS4W - YP(2)*YP(2)
     1 /Y(2))/Y(2) - CS5)*Y(3) + ICS6W
      GO TO 10
      ENTRY F4 (Y,YP)
C SUBROUTINE FOR G IN REGION INBOARD OF ORIFICES
      YP(2)= 0.
      YP(4) = (CS5 - ICS4W/Y(2))*Y(3) + ICS6W
10    YP(1)= 1.
      YP(3) = Y(4)
      YP(5) = Y(3)
      RETURN
      END
```

```
$IBFTC RKGHC

      SUBROUTINE RKGC (DERIV, Y, XFINAL, DELTA, Q, YP, N)
C  RUNGE-KUTTA-GILL INTEGRATION OF N-1 COMPLEX FUNCTIONS OF COMPLEX
C  ARGUMENT Y(1) FROM Y(1)INITIAL TO XFINAL
      DIMENSION A(4), B(4), C(4)
      COMPLEX Y(1), Q(1), YP(1), XFINAL, DELTA, T
      DATA A/.5, .292893219, 1.70710678, .166666667/, B/2., 1., 1., 2./,
     1     C/.5, .292893219, 1.70710678, .5/
      KK = CABS((XFINAL-Y(1))/DELTA) + .01
      IF (KK.LE.0) GO TO 20
      DO 5 I = 1, N
5     Q(I)=0.
      DO 10 K = 1, KK
      DO 10 J = 1, 4
      CALL DERIV(Y,YP)
      DO 10 I=1,N
      T=A(J)*(YP(I)-B(J)*Q(I))
      Y(I)=Y(I)+DELTA*T
10    Q(I)=Q(I)+3.*T-C(J)*YP(I)
20    RETURN
      END
```

REFERENCES

1. Vohr, J. H.; and Chow, C. Y.: Characteristics of Herringbone-Grooved, Gas-Lubricated Journal Bearings. J. Basic Eng., vol. 87, no. 3, Sept. 1965, pp. 568-578.

2. Rieger, N. F., ed.: Design of Gas Bearings. Vol. I: Design Notes. Mechanical Technology, Inc., 1966.

3. Cunningham, Robert E.; Fleming, David P.; and Anderson, William J.: Experimental Stability Studies of the Herringbone-Grooved Gas-Lubricated Journal Bearing. J. Lubr. Tech., vol. 91, no. 1, Jan. 1969, pp. 52-59.

4. Fleming, David P.; Cunningham, Robert E.; and Anderson, William J.: Stability Analysis for Unloaded Externally Pressurized Gas-Lubricated Bearings with Journal Rotation. NASA TN D-4934, 1968.

5. Lund, J. W.: The Hydrostatic Gas Journal Bearing with Journal Rotation and Vibration. J. Basic Eng., vol. 86, no. 2, June 1964, pp. 328-336.

6. Lund, J. W.: A Theoretical Analysis of Whirl Instability and Pneumatic Hammer for a Rigid Rotor in Pressurized Gas Journal Bearings. J. Lubr. Tech., vol. 89, no. 2, Apr. 1967, pp. 154-166.

7. Pan, C. H. T.: Spectral Analysis of Gas Bearing Systems for Stability Studies. Dynamics and Fluid Mechanics. Vol. 3, Part 2 of Developments in Mechanics. T. C. Huang and M. W. Johnson, Jr., eds., John Wiley & Sons, Inc., 1965, pp. 431-447.

"The aeronautical and space activities of the United States shall be conducted so as to contribute . . . to the expansion of human knowledge of phenomena in the atmosphere and space. The Administration shall provide for the widest practicable and appropriate dissemination of information concerning its activities and the results thereof."

—NATIONAL AERONAUTICS AND SPACE ACT OF 1958

NASA SCIENTIFIC AND TECHNICAL PUBLICATIONS

TECHNICAL REPORTS: Scientific and technical information considered important, complete, and a lasting contribution to existing knowledge.

TECHNICAL NOTES: Information less broad in scope but nevertheless of importance as a contribution to existing knowledge.

TECHNICAL MEMORANDUMS: Information receiving limited distribution because of preliminary data, security classification, or other reasons.

CONTRACTOR REPORTS: Scientific and technical information generated under a NASA contract or grant and considered an important contribution to existing knowledge.

TECHNICAL TRANSLATIONS: Information published in a foreign language considered to merit NASA distribution in English.

SPECIAL PUBLICATIONS: Information derived from or of value to NASA activities. Publications include conference proceedings, monographs, data compilations, handbooks, sourcebooks, and special bibliographies.

TECHNOLOGY UTILIZATION PUBLICATIONS: Information on technology used by NASA that may be of particular interest in commercial and other non-aerospace applications. Publications include Tech Briefs, Technology Utilization Reports and Notes, and Technology Surveys.

Details on the availability of these publications may be obtained from:

SCIENTIFIC AND TECHNICAL INFORMATION DIVISION

NATIONAL AERONAUTICS AND SPACE ADMINISTRATION

Washington, D.C. 20546